iScience

CellPress
OPEN ACCESS

Article

Prevention of Chromatin Destabilization by FACT Is Crucial for Malignant Transformation

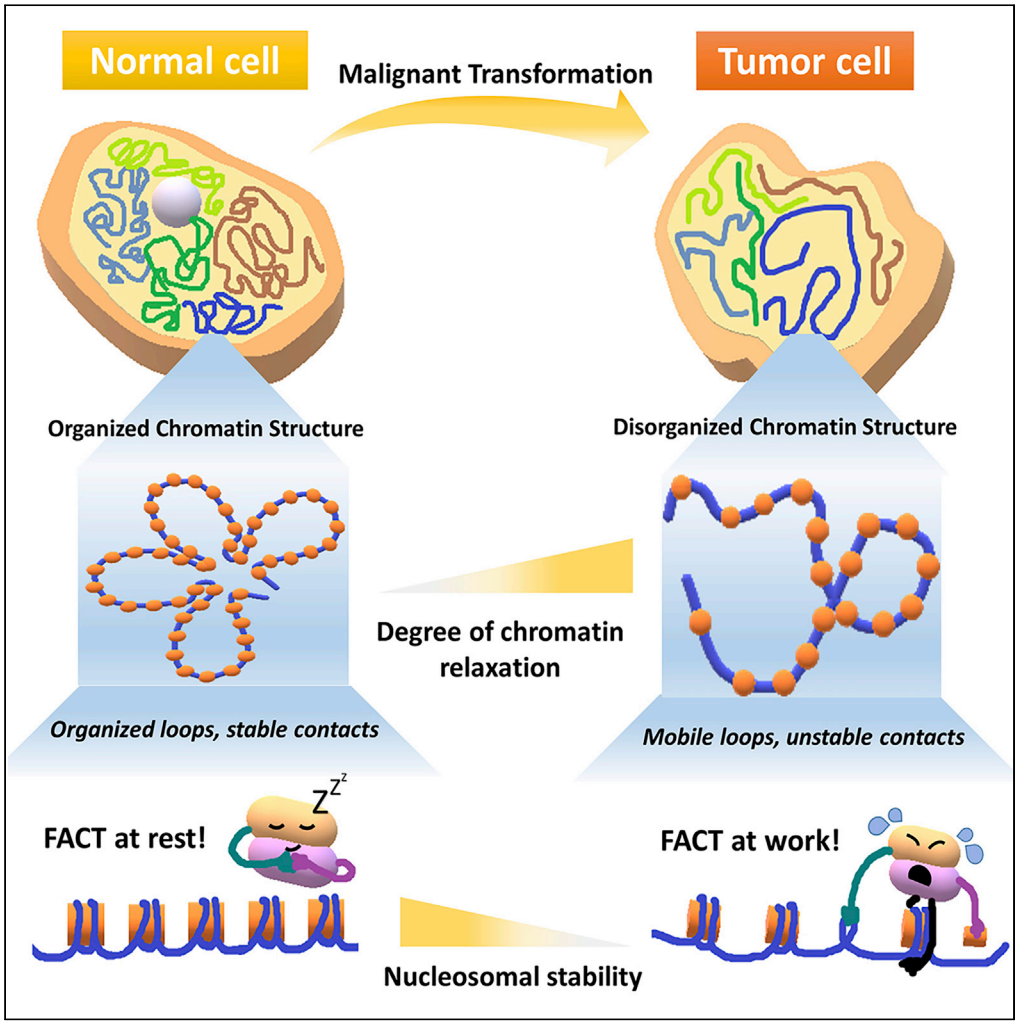

Poorva Sandlesh, Alfiya Safina, Imon Goswami, ..., Eduardo C. Gomez, Jianmin Wang, Katerina V. Gurova

katerina.gurova@roswellpark.org

HIGHLIGHTS

FACT is essential for viability of the tumor, but not for normal cells

FACT level depends on transcription, but transcription does not depend on FACT

FACT preserves nucleosomes during transcription to maintain chromatin integrity

FACT maintains chromatin in destabilized state during malignant transformation

Sandlesh et al., iScience *23*, 101177
June 26, 2020
https://doi.org/10.1016/j.isci.2020.101177

iScience

CellPress
OPEN ACCESS

Article

Prevention of Chromatin Destabilization by FACT Is Crucial for Malignant Transformation

Poorva Sandlesh,[1,4] Alfiya Safina,[1] Imon Goswami,[1] Laura Prendergust,[1,5] Spenser Rosario,[2] Eduardo C. Gomez,[3] Jianmin Wang,[3] and Katerina V. Gurova[1,6,*]

SUMMARY

Histone chaperone FACT is commonly expressed and essential for the viability of transformed but not normal cells, and its expression levels correlate with poor prognosis in patients with cancer. FACT binds several components of nucleosomes and has been viewed as a factor destabilizing nucleosomes to facilitate RNA polymerase passage. To connect FACT's role in transcription with the viability of tumor cells, we analyzed genome-wide FACT binding to chromatin in conjunction with transcription in mouse and human cells with different degrees of FACT dependence. Genomic distribution and density of FACT correlated with the intensity of transcription. However, FACT knockout or knockdown was unexpectedly accompanied by the elevation, rather than suppression, of transcription and with the destabilization of chromatin in transformed, but not normal cells. These data suggest that FACT stabilizes and reassembles nucleosomes disturbed by transcription. This function is vital for tumor cells because malignant transformation is accompanied by chromatin destabilization.

INTRODUCTION

Multiple chromatin alterations are found in cancer, such as mutations and changes in the expression of histones, chromatin remodeling factors, histone chaperones, and enzymes that post-translationally modify histones (reviewed in Ferraro, 2016; Flavahan et al., 2017; Morgan and Shilatifard, 2015). The benefits that these alterations provide to tumor cells are unclear. The prevailing hypothesis is that these alterations lead to changes in the expression of genes that promote cell growth or inhibit differentiation and cell death. However, this hypothesis is not completely satisfying because it does not explain how chromatin alterations (e.g., mutations in core histones) with extensive genome-wide effects can lead to changes in the transcription of specific genes that are beneficial for cancer cells.

One example of such an alteration is the frequent overexpression of histone chaperone FACT (Facilitates Chromatin Transcription) in multiple human tumors (Carter et al., 2015; Ding et al., 2016; Fleyshman et al., 2017; Garcia et al., 2013). FACT consists of two subunits in higher eukaryotes: Structure Specific Recognition Protein 1 (SSRP1) and Suppressor of Ty 16 (SPT16). Both subunits are highly conserved in all eukaryotes and perform similar functions. They interact with all components of the nucleosome (i.e., histone oligomers and DNA) and are involved in replication, transcription, and DNA repair (reviewed in Gurova et al., 2018). FACT is not only overexpressed in different types of tumors but also associated with poor prognosis (Carter et al., 2015; Garcia et al., 2013; Attwood et al., 2017; Dermawan et al., 2016). Moreover, genetic or chemical inhibition of FACT has strong anti-cancer effects in multiple cancer models (Carter et al., 2015; Garcia et al., 2013; Dermawan et al., 2016; Gasparian et al., 2011). At the same time, mammalian FACT is not expressed or is expressed at much lower levels in non-tumor cells *in vitro* and in differentiated cells *in vivo* (Garcia et al., 2011). Inhibition of FACT in FACT-positive normal cells has little effect on cell growth or viability (Garcia et al., 2013; Mylonas and Tessarz, 2018; Kolundzic et al., 2018). These findings suggest that FACT may be a promising target for anti-cancer treatment. However, how FACT supports the viability of tumor cells is unclear.

In cell-free experiments, FACT was essential for transcription elongation through nucleosomal DNA (Orphanides et al., 1998, 1999). Based on these data, when we first noticed that FACT was enriched at coding regions of so-called pro-cancerous genes (i.e., genes involved in cell proliferation, response to stress, and maintenance of pluripotency) (Garcia et al., 2013), we assumed that FACT was involved in the transcription

[1]Department of Cell Stress Biology, Roswell Park Comprehensive Cancer Center, Carlton and Elm Streets, Buffalo, NY 14127, USA

[2]Department of Cancer Genetics, Roswell Park Comprehensive Cancer Center, Carlton and Elm Streets, Buffalo, NY 14127, USA

[3]Department of Bioinformatics, Roswell Park Comprehensive Cancer Center, Carlton and Elm Streets, Buffalo, NY 14127, USA

[4]Present address: Division of Reproductive Science in Medicine, Department of Obstetrics and Gynecology, Robert H. Lurie Comprehensive Cancer Center, Feinberg School of Medicine, Northwestern University, Chicago, IL 60611.

[5]Present adress: Department of Biochemistry and Molecular Pharmacology, New York University, New York, NY, 10016, USA

[6]Lead Contact

*Correspondence: katerina.gurova@roswellpark.org

https://doi.org/10.1016/j.isci.2020.101177

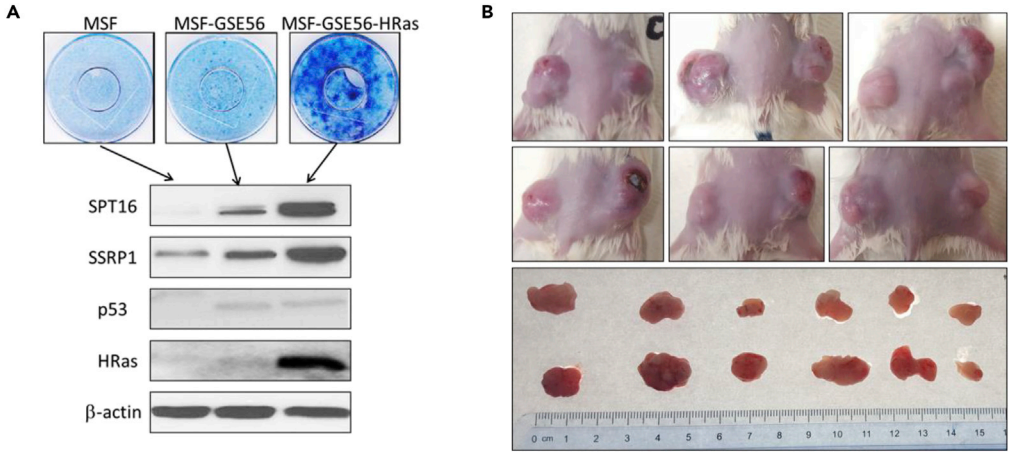

Figure 1. Development of Conditional *Ssrp1* Knockout Cell Model with Different Basal Levels of FACT

(A) Primary (Pr) mouse skin fibroblasts (MSFs) were isolated from tail tips of *Ssrp1*$^{fl/fl}$;*CreERT*$^{2+/+}$ mice and transduced with GSE56 to become immortalized (Im) or GSE56 and HRas^{V12} oncogene to become transformed (Tr). (Top) Methylene blue staining of plates with corresponding cells at confluency. (Bottom) Western blotting of the lysates of the corresponding cells probed with the indicated antibodies.

(B) Growth of Tr cells in severe combined immunodeficiency mice. Representative photographs of mice and tumors on day 32 after inoculation of transformed cells.

elongation of these genes, many of which are essential for tumor growth. However, there were many unclear issues with this interpretation. Several groups recently reported that mammalian FACT could not bind the folded nucleosome (Carvalho et al., 2013; Erkina and Erkine, 2015; Safina et al., 2013; Tsunaka et al., 2016; Wang et al., 2018), which makes it difficult to explain how FACT can remove the nucleosomal barrier for transcription and replication. It is also unclear how FACT selects genomic regions because it does not have sequence-specific DNA binding or histone modification "reader" domains. If the elongating RNA polymerases recruited FACT, then why would its inhibition be much more toxic for tumor than normal cells? Furthermore, depletion of FACT from tumor cells, which were the most sensitive to FACT knockdown, did not result in the inhibition of the expression of "pro-cancerous" genes (Fleyshman et al., 2017). Similarly, it was recently shown that there was no inhibition of the transcription of FACT-enriched genes in mouse embryonic stem cells or human fibroblasts (Mylonas and Tessarz, 2018; Kolundzic et al., 2018).

The aim of this study was to compare the effect of FACT loss in syngeneic mammalian cells at different stages of tumorigenic transformation to understand whether FACT has special function in transformed and tumor cells.

RESULTS

Development of Conditional *Ssrp1* Knockout Cell Model with Different Basal Levels of FACT

Previously, we observed that tumor cells express higher levels of the FACT subunits and their viability is more dependent on FACT expression than primary or immortalized non-tumor cells (Garcia et al., 2011, 2013; Gurova et al., 2018). To understand the mechanism of this difference in FACT dependency, we generated isogenic cells from mouse skin fibroblasts (MSFs) isolated from *Ssrp1*$^{fl/fl}$;*CreER*$^{T2+/+}$ mice, in which the *Ssrp1* gene can be deleted by tamoxifen treatment (Sandlesh et al., 2018). As a negative control, we used cells from *Ssrp1*$^{fl/+}$;*CreER*$^{T2+/+}$ mice because deletion of one allele of *Ssrp1* did not affect the mouse phenotype (Cao et al., 2003). We previously demonstrated that depletion of SSRP1 leads to an efficient and rapid loss of both SSRP1 and SPT16 proteins (Safina et al., 2013). Thus, the whole FACT complex can be eliminated from these cells by the administration of the active metabolite of tamoxifen, 4-hydroxytamoxifen (4-OHT).

Primary MSFs are highly sensitive to contact inhibition, survive in culture for four to five passages, and then undergo replicative senescence. The MSFs were transduced with the genetic suppressor element (GSE) 56, an inhibitor of tumor suppressor p53 (Ossovskaya et al., 1996). MSF-GSE56 cells became

immortal but were still sensitive to contact inhibition (Figure 1A), did not grow in semisolid medium, and did not form tumors in mice. MSF-GSE56 cells were subsequently transduced with the mutant H-Ras^{V12} oncogene. These cells (MSF-GSE56-HRas) lost contact inhibition and formed foci in dense culture (Figure 1A). They also grew in semisolid medium and quickly developed aggressive tumors in mice (Figure 1B), i.e., acquired a fully transformed phenotype. The primary MSFs had low but detectable levels of SSRP1 and SPT16, which were elevated in immortalized MSF-GSE56 cells and further increased in the transformed MSF-GSE56-HRas cells (Figure 1A). In all experiments, we used primary cell cultures isolated from two to four individual mice as biological replicates, which were independently immortalized and then transformed as described earlier. The main figures include the mean data for all tested cell variants or representative images. Data for additional cell variants are available in the supplementary materials. Cultures of immortalized and transformed cells generated from the same primary cells are labeled with the same number.

Loss of FACT Compromises Replication and Causes Death of Transformed but Not Primary Normal Cells

4-OHT administration resulted in the disappearance of *Ssrp1* mRNA and SSRP1 and SPT16 proteins between days 3 and 5 after the start of treatment (Figures 2A, S1A, and S1B). 4-OHT treatment did not affect the growth of primary cells but led to significant reduction in the number of the transformed and, to a lesser extent, the immortalized cells compared with untreated control (Figures 2B and S1C). Importantly, tumors that formed from the transformed cells in severe combined immunodeficiency mice quickly disappeared after the administration of tamoxifen to mice (Figures 2C and S2).

To figure out whether FACT-depleted immortalized and transformed cells stop growing or die we first analyzed cell cycle using flow cytometry. The cell cycle distribution of the primary cells remained unchanged following 4-OHT treatment, whereas transformed and, to a lesser extent, immortalized, cells were accumulated in the S and G2/M phases (Figures 2D and S3). At the same time the proportion of cells with ongoing DNA replication, as judged by incorporation of 5-ethynyl-2′-deoxyuridine (EdU), was reduced in transformed and immortalized cells after FACT depletion (Figures 2E and S1D). The combination of accumulation of cells in S-phase with reduced proportion of cells capable of DNA synthesis suggests that FACT loss leads to the block of DNA replication in transformed and immortalized cells. The increased proportion of cells in the G2/M phase suggests activation of G2 checkpoint or difficulty in passing through mitosis, what may occur when mitosis starts in cells with unfinished replication or unresolved homologous recombination. There are data showing the functional role of FACT in DNA replication and homologous recombination (reviewed in Gurova et al., 2018). The marker of these events is anaphase bridges (Fragkos and Naim, 2017). There was significantly elevated number of anaphase bridges after FACT depletion in the transformed, but not in primary, cells (Figure 2F). There was also increase in the number of anaphase bridges upon FACT depletion in immortalized cells, but the difference did not reach statistical significance. Thus, we concluded that whereas FACT loss has minimal effects in primary cells, in transformed, and to a lesser degree in immortalized, cells, it causes problem with DNA replication, leading to the occurrence of mitosis in cells with not fully replicated DNA. Eventually, cells with significant problems with replication should die and in line with this notion, we also detected activated caspase 3/7 after 4-OHT administration in transformed, and in one of three replicates of immortalized, cells, but not in primary cells (Figures 2G and S4). 4-OHT did not cause any of these effects in cells obtained from mice heterozygous for *Ssrp1*^{fl} allele (Figures 2, S1, and S3).

Together, these data suggest that FACT loss compromises growth of immortalized and viability of transformed cells. Importantly, the difference in the FACT dependence of cells cannot be explained by the difference in cell proliferation because in basal conditions, immortalized and transformed cells had similar cell cycle profiles and the same number of EdU-positive cells in the populations (Figures S1D and S3).

Effects of FACT Inactivation on Transcription

The problem observed with replication in transformed and immortalized cells following FACT removal may be due to the direct involvement of FACT in replication or because of the loss of FACT-dependent transcription of genes, whose products support replication. We previously observed the binding of FACT to chromatin of genes involved in replication and cell cycle in human tumor cells (Fleyshman et al., 2017; Garcia et al., 2013).

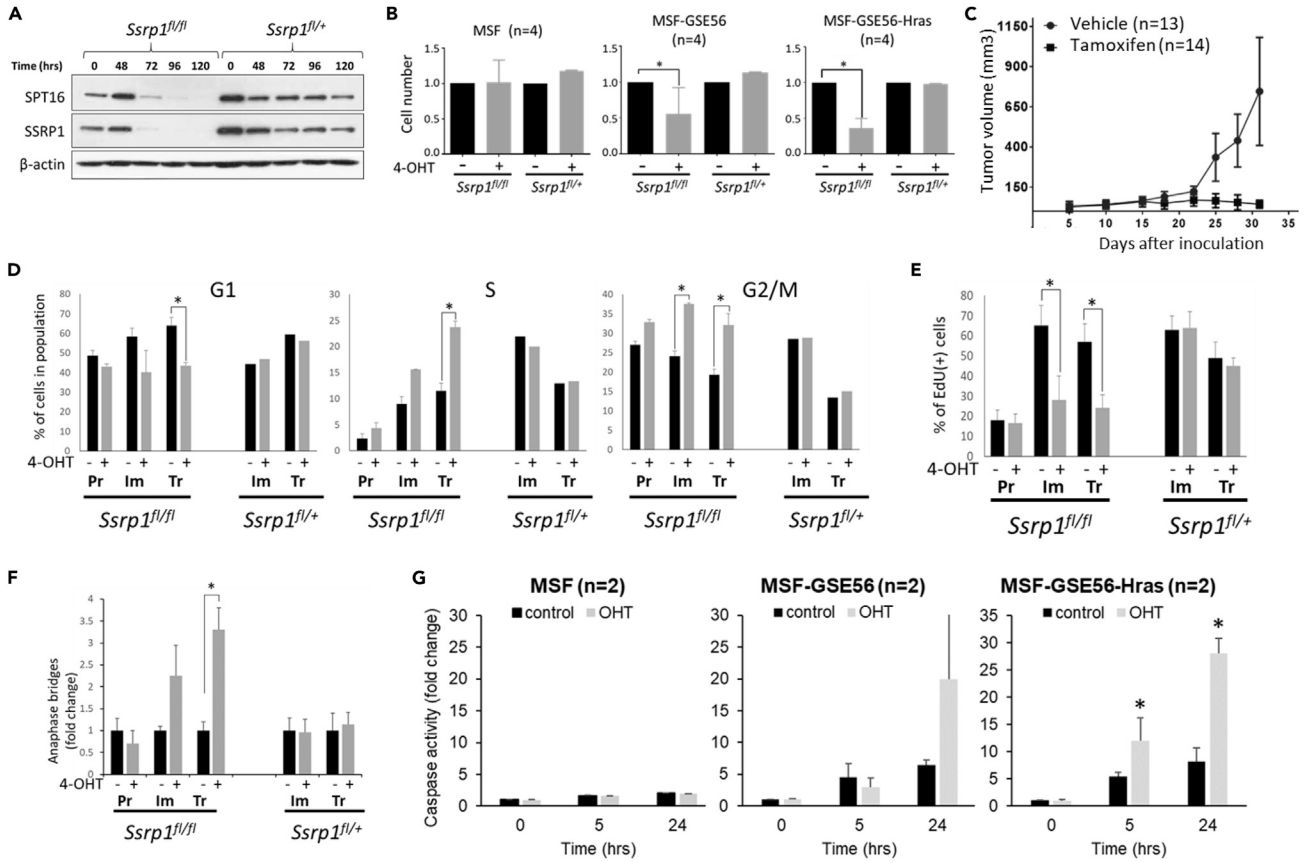

Figure 2. Different Consequences of FACT Depletion in Primary (Pr), Immortalized (Im), and Transformed (Tr) Cells

(A) Excision of *Ssrp1*$^{fl/fl}$ results in disappearance of SSRP1 and SPT16 proteins after 4 days of treatment with 4-OHT. Western blotting of extracts of Im cells at indicated time points after start of treatment with 4-OHT probed with the indicated antibodies.

(B) Viability of Pr, Im, and Tr cells with and without FACT. All cells were plated at equal numbers after the end of treatment with 4-OHT (5 days). 2 days later the relative number of cells was assessed using resazurin/resorufin cell viability assay. Bars are means of four cell lines, isolated from individual mice of each genotype ± SD (see Figure S1C for data of individual cell lines).

(C) Growth of Tr cells in severe combined immunodeficiency mice treated with tamoxifen or vehicle. Average tumor volume ± SD. (See also Figure S2).

(D) Quantitation of the cell cycle distribution data obtained from cells replated at the end of 4-OHT treatment and grown for 24 h. Bars are means of two cell lines isolated from individual mice ± SD (see Figure S3 for each cell line).

(E) EdU incorporation into different cells treated or not with 4-OHT. Bars are means of two cell lines ± SD (see Figure S1D for each cell line).

(F) Normalized average number of anaphase bridges per number of mitosis. Bars are mean of two cell lines ± SD. Control cells of each variant = 1.

(G) Activities of caspases 3 and 7 in the cells with and without 4-OHT treatment assessed at the moment (0 h) and at different time points after caspase substrate addition. Bars are means of two replicates of two cell cultures of each genotype ± SD (see Figure S4 for each cell line). *p < 0.05.

To discriminate between these scenarios, we assessed the effect of FACT inactivation on global transcription, using the 5-ethynyluridine (EU) incorporation assay, and on transcription of individual genes using next-generation sequencing (NGS) of RNA isolated from cells (RNA sequencing [RNA-seq]). Surprisingly, the EU incorporation was increased following *Ssrp1* knockout (KO) in immortalized and transformed cells, but not changed in primary cells (Figures 3A and S5).

For RNA-seq, we used cells from *Ssrp1*$^{fl/fl}$;*CreER*$^{T2+/+}$ and *Ssrp1*$^{+/+}$; *CreER*$^{T2+/+}$ mice to filter out the effect of 4-OHT administration and Cre activation, independent of *Ssrp1* KO. Two biological replicates were used for each condition, and their correlation was >98% (>99% in 11 of 12 cases, Figure S6). Principal-component analysis (PCA) confirmed the similarity of all replicates (Figure 3B). In addition, PCA showed that all primary samples were clustered together independently of their *Ssrp1* alleles. 4-OHT had little effect on the primary cells of either genotype (Figure 3B). The immortalized and transformed samples diverged from the primary MSFs in two directions: samples from cells with wild-type *Ssrp*1 were found along principal

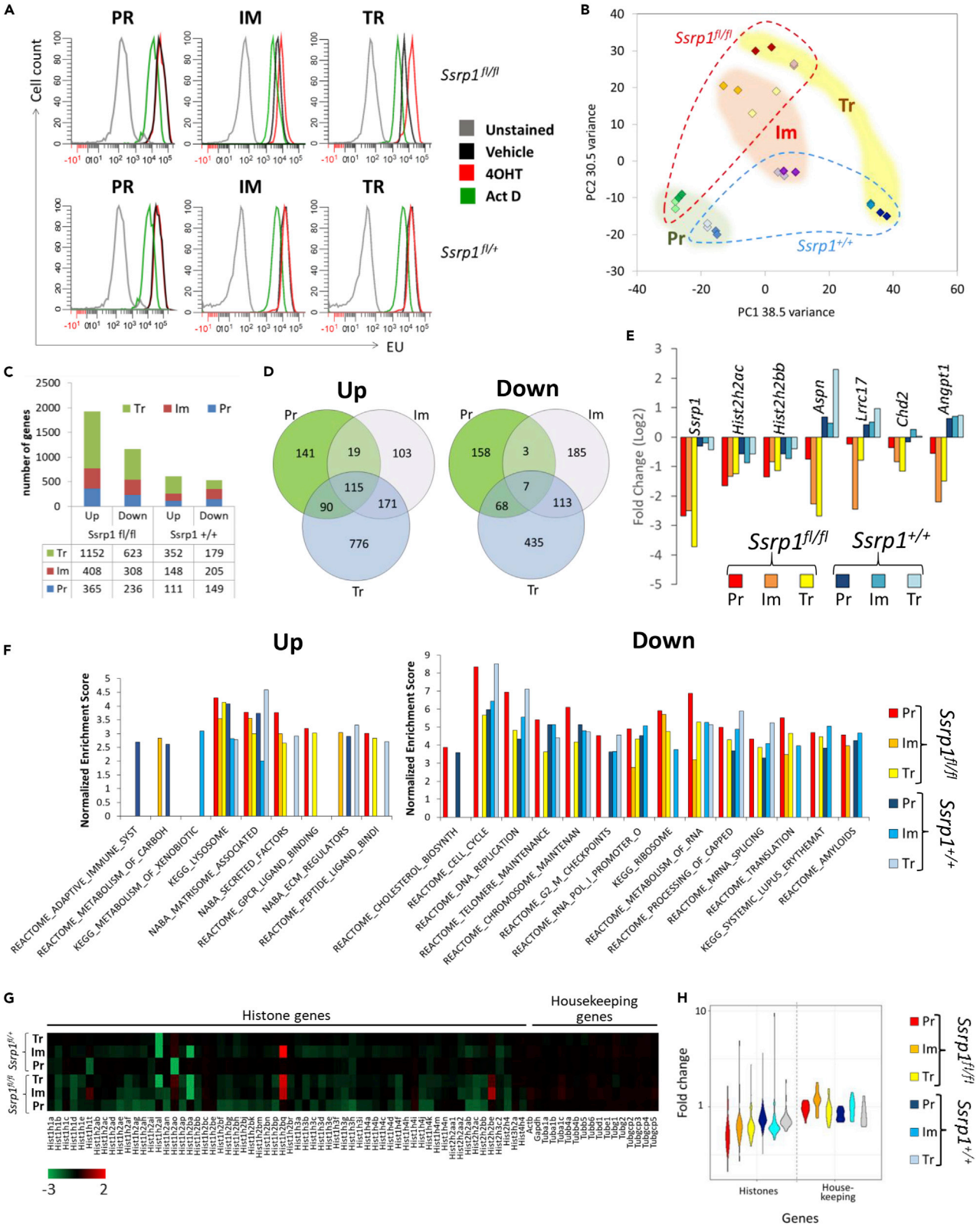
A
PR
IM
TR
Cell count
EU
Ssrp1fl/fl
Ssrp1fl/+
Unstained
Vehicle
4OHT
Act D
B
PC2 30.5 variance
PC1 38.5 variance
Ssrp1fl/fl
Ssrp1+/+
Tr
Im
Pr
C
number of genes
Tr
Im
Pr
Up
Down
Ssrp1 fl/fl
Ssrp1 +/+
Tr 1152 623 352 179
Im 408 308 148 205
Pr 365 236 111 149
D
Up
Down
Pr
Im
Tr
141
19
103
115
90
171
776
158
3
185
7
68
113
435
E
Fold Change (Log2)
Ssrp1
Hist2h2ac
Hist2h2bb
Aspn
Lrrc17
Chd2
Angpt1
Ssrp1fl/fl
Ssrp1+/+
F
Up
Down
Normalized Enrichment Score
REACTOME_ADAPTIVE_IMMUNE_SYST
REACTOME_METABOLISM_OF_CARBOH
KEGG_METABOLISM_OF_XENOBIOTIC
KEGG_LYSOSOME
NABA_MATRISOME_ASSOCIATED
NABA_SECRETED_FACTORS
REACTOME_GPCR_LIGAND_BINDING
NABA_ECM_REGULATORS
REACTOME_PEPTIDE_LIGAND_BINDI
REACTOME_CHOLESTEROL_BIOSYNTH
REACTOME_CELL_CYCLE
REACTOME_DNA_REPLICATION
REACTOME_TELOMERE_MAINTENAN
REACTOME_CHROMOSOME_MAINTENAN
REACTOME_G2_M_CHECKPOINTS
REACTOME_RNA_POL_I_PROMOTER_O
KEGG_RIBOSOME
REACTOME_METABOLISM_OF_RNA
REACTOME_PROCESSING_OF_CAPPED
REACTOME_MRNA_SPLICING
REACTOME_TRANSLATION
KEGG_SYSTEMIC_LUPUS_ERYTHEMAT
REACTOME_AMYLOIDS
Pr
Im
Tr
Ssrp1fl/fl
Ssrp1+/+
G
Histone genes
Housekeeping genes
Ssrp1fl/fl
Ssrp1+/+
Tr
Im
Pr
-3
2
H
Fold change
Histones
House-keeping
Genes
Pr
Im
Tr
Ssrp1fl/fl
Ssrp1+/+

Figure 3. Effects of FACT Inactivation on Transcription in Primary (Pr), Immortalized (Im) and Transformed (Tr) Mouse Cells

(A) EU incorporation into Pr, Im, and Tr cells of two genotypes treated or untreated with 4-OHT for 5 days. As control cells without EU and cells treated with transcription inhibitor actinomycin D (Act D) were used. Data for one cell line of each genotype are shown. Other cell lines are shown in Figure S5.

(B–H) Analyses of two biological replicates of paired-end RNA-seq samples of Pr, Im, and Tr homozygous wild-type or floxed *Ssrp1* cells treated or untreated with 4-OHT. Correlation between replicates is shown in Figure S6. (B) Principle-component analysis. Darker colors, 4-OHT; lighter colors, control samples. (C) Number of up- and downregulated genes. Fold change (FC) > ±1.5, adjusted p value <0.05. Table shows number of genes in each category. (D) Commonly or differentially up- and downregulated genes in Pr, Im, and Tr cells with floxed *Ssrp1* upon 4-OHT treatment. Venn diagrams for wild-type *Ssrp1* cells are shown in Figure S7A. (E) Fold change (FC) of expression of genes commonly downregulated in Pr, Im, and Tr cells with floxed *Ssrp1* upon 4-OHT treatment. (F) Summary of GSEA. Normalized enrichment scores (NES) are shown for all significantly enriched gene lists in Pr, Im, or Tr cells of either of genotypes. Individual NES plots are shown in Figure S7B. (G) Heat plot demonstrating FC of expression of replication-dependent histones and several housekeeping genes in different conditions between 4-OHT-treated and untreated cells. (H) Violin plots of FC of expression of all replication-dependent histones and selected housekeeping genes, shown in (G) between 4-OHT-treated and untreated cells.

component 1 (PC1) (38.5% variance), and samples from cells with floxed *Ssrp1* alleles were found along PC2 (30.5% variance). The 4-OHT-treated samples from immortalized and transformed cells with floxed *Ssrp1* were clearly separated from the untreated samples, but the impact of 4-OHT administration on the distribution of these samples was very modest and shifted the immortalized and transformed cells with floxed *Ssrp1* alleles closer to the position of the primary cells along PC1 (Figure 3B). Thus, PCA showed that transcription of genes was changed much stronger due to immortalization and transformation, than due to *Ssrp1* KO. The changes were of a rather random nature as there was a high variance between independently generated immortalized and transformed cells. Because the differences were observed even before *Ssrp1* deletion, it cannot be attributed to FACT inactivation. In line with the phenotypic studies, FACT inactivation had a more prominent effect on gene expression in transformed and immortalized cells than in primary cells.

4-OHT administration altered gene expression in cells of both genotypes with floxed and wild-type *Ssrp1*, and there was significant overlap in downregulated genes in primary cells between the two genotypes (Figure S7), suggesting that the effect of 4-OHT is comparable in these cells with *Ssrp1* deletion. In all cell variants with floxed *Ssrp1* there were more upregulated than downregulated genes upon 4-OHT administration. In contrast, in cells with wild-type *Ssrp1* there were similar numbers of up- and downregulated genes (Figures 3C and S7A). There were 115 genes commonly upregulated across all three cell types following Ssrp1 KO but only 7 that were downregulated (Figure 3D). The most significantly and specifically (i.e., only in *Ssrp1*-floxed but not wild-type cells) downregulated gene was *Ssrp1* itself (Figure 3E). The commonly up- or downregulated genes did not belong to any known gene sets based on gene set enrichment analysis (GSEA).

Surprisingly, when we performed GSEA on genes up- or downregulated after 4-OHT administration in each type of both genotypes, we obtained very similar lists of genes in all cases (Figures 3F and S7B), suggesting that 4-OHT administration and Cre activation, but not *Ssrp1* KO, might be the major driver of the gene expression changes. No functional gene categories responded to *Ssrp1* KO exclusively in the cells in which we observed strong phenotypic changes (i.e., immortalized and transformed cells with floxed *Ssrp1*). There was significant enrichment of genes involved in cell cycle-related processes (e.g., DNA replication, telomeres, and chromosome maintenance) among genes downregulated by 4-OHT. However, their expression was reduced in both *Ssrp1* floxed and wild-type cells, although this effect was stronger in cells with *Ssrp1* floxed than wild-type alleles. For example, expression of the replication-dependent histone genes, which are highly expressed during the S-phase of the cell cycle, was reduced to a greater extent in *Ssrp1* floxed cells than in *Ssrp1* wild-type cells (Figures 3G and 3H), which is consistent with the observed phenotypic changes. However, the strongest reduction was observed in primary cells in which we saw no difference in growth or cell cycle distribution upon 4-OHT treatment.

Identification of transcriptional changes in the similar gene lists upon FACT loss in different cells combined with the low number of commonly changed genes suggests that changes in gene expression may be secondary to FACT loss, i.e., in response to dysregulation of certain processes (e.g., replication) rather than direct FACT involvement in the transcription of individual genes. To assess the direct role of FACT in the regulation of expression of individual genes, we calculated correlation between the level of FACT enrichment at a gene, transcription of this gene in basal conditions, and changes in expression of this gene upon *Ssrp1* KO. For this we performed chromatin immunoprecipitation with an SSRP1 antibody followed by NGS (chromatin immunoprecipitation sequencing [ChIP-seq]) in immortalized and transformed cells. The level of FACT in the primary cells was too low to accurately run this assay. We observed SSRP1 enrichment at coding regions of genes in proportion to the level of transcription of these genes (Figure 4A).

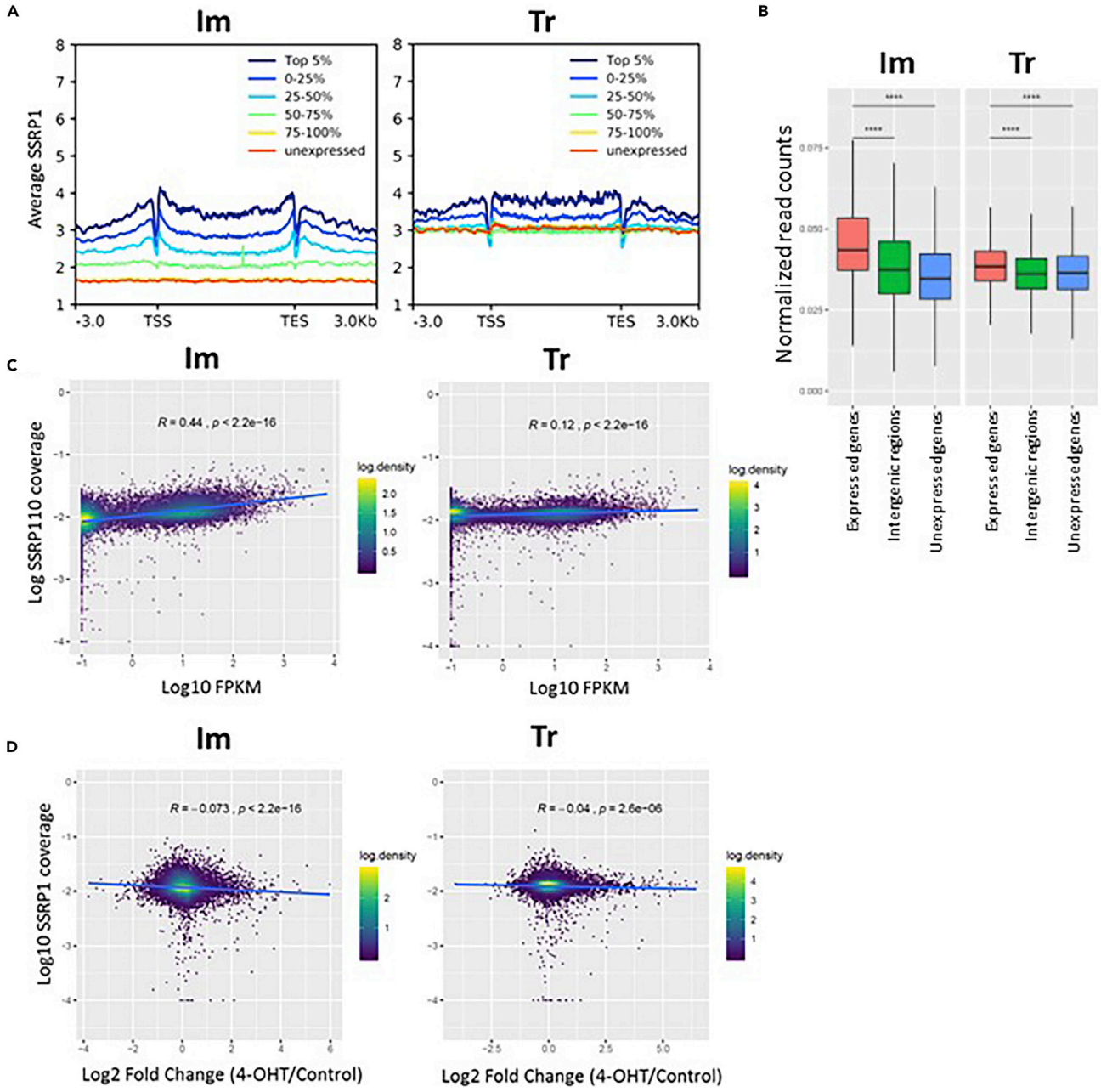

Figure 4. Relationship between FACT Genomic Distribution and Transcription in Mouse Cells (*Ssrp1*$^{fl/fl}$; *CreER*$^{T2+/+}$ #2)

Data for other cell lines are shown on Figures S8 and S9.

(A) Average enrichment of SSRP1 (ChIP-seq) at genes depending on the levels of their transcription defined by RNA-seq read density in basal conditions.

(B) Whisker plot of normalized FACT enrichment at different categories of genomic regions.

(C) Dot plot demonstrating relationship between SSRP1 enrichment and transcription.

(D) Dot plot demonstrating relationship between SSRP1 enrichment and fold change in gene expression upon *Ssrp1* KO. R, Pearson correlation coefficient.

In immortalized cells, this dependence was stronger than in transformed cells. There was higher level of SSRP1 everywhere, including non-transcribed regions and genes expressed at low levels in transformed cells (Figures 4A and 4B). This pattern was reproduced with independently generated immortalized and transformed cell cultures from a different mouse and using a different platform for RNA-seq (Figure S8, see details in Transparent Methods). In line with this, significant positive correlation between SSRP1 and RNA read coverage under basal conditions was much stronger in immortalized than transformed cells

(Pearson correlation coefficients 0.44 versus 0.12, Figures 4C and S9A). However, the distribution of nucleosomes in basal conditions measured using histone H3 ChIP-seq was not significantly different between the two cell types (Figure S8).

Next, we looked whether genes that are occupied by FACT would have stronger changes in their transcription upon FACT removal than genes that were not occupied by FACT in basal conditions. For this we assessed correlation between FACT enrichment (SSRP1 ChIP-seq reads) and FACT dependence (fold change of transcription between cells treated with 4-OHT and control cells). In all cases, we saw negative correlation between FACT enrichment and FACT dependence (Figures 4D, S9B, and S9C). These correlations were highly significant and stronger for immortalized cells than for transformed cells, i.e., loss of FACT led to a stronger increase in gene expression in immortalized cells than in transformed cells, suggesting that the presence of FACT might interfere with gene transcription, and this effect is weakened in transformed cells.

Cell-free experiments showed that the absence of FACT caused RNA polymerase II to pause at several positions within the nucleosome and, therefore, produce early terminated short transcripts (Hsieh et al., 2013). In addition, several studies in yeast demonstrated that inhibition of FACT was associated with the loss of nucleosomes at the coding regions of genes (Erkina and Erkine, 2015; Feng et al., 2016; Morillo-Huesca et al., 2010; Myers et al., 2011), which might lead to cryptic intra-genic initiation. In both cases, non-functional transcripts (i.e., early terminated or incorrectly initiated) might mask the presence of proper full-length transcripts when analyzed using NGS (short reads) or total EU incorporation. However, both types of short transcripts could skew the distribution of reads along the coding region: early termination could generate bias toward an overrepresentation of reads corresponding to the 5′ versus 3′ exons; cryptic initiation could result in an overrepresentation of reads from the 3′ exons. Therefore, we compared the number of reads representing individual exons between samples in the presence or absence of FACT and observed increase in 5′ UTR exons in immortalized and transformed cells lacking FACT (Figures 5A and 5B). Furthermore, we observed a significant increase in the proportion of reads corresponding to introns in transformed and, to a lesser degree, immortalized cells (Figures 5A, 5C, S10A, and S10B). This so-called intron retention was previously observed in tumor cells (Smart et al., 2018; Dvinge and Bradley, 2015) and was thought to be the result of mutations in splicing factors (Wong et al., 2016). However, it can also be explained by cryptic initiation from introns due to the loss of nucleosomes. Because we detected "intron retention" in all independently transformed cell cultures concomitant with other signs of chromatin destabilization, we propose that the second explanation is more probable.

Another important difference between cells of different types noticed in the process of analysis of the RNA-seq data was significant changes in the proportion of reads mapped to annotated genomic regions versus regions with no features (i.e., lacking any known transcripts or regulatory elements) between primary, immortalized, and transformed cells independently of genotype and 4-OHT treatment (Figures 5D and 5E). There were significantly more reads with no features in immortalized and transformed cells compared with the primary cells. The appearance of these reads may suggest either contamination of RNA with genomic DNA or that the samples contained elevated levels of products of so-called pervasive transcription from non-coding genomic regions due to the loss of chromatin packaging at these regions (Loonstra et al., 2001). Because the RNA was isolated simultaneously using the same method for all types of cells, the first explanation (i.e., genomic DNA contamination) seems less probable. However, to exclude this possibility, we analyzed the samples from independently isolated immortalized, and transformed cells from mice with floxed *Ssrp1* using a different method of RNA isolation (Trizol reagent versus purification column) and sequencing platform (single versus paired-end reads). The data generated were consistent with the first set of data (Figures S10C and S10D).

Effect of FACT Inactivation on Transcription in Human Cells

To confirm these findings in human cells, we examined the relationship between FACT and gene expression in fibrosarcoma cell line HT1080 for which we already had SSRP1 ChIP-seq data from two independent experiments of two to three replications and data from several gene expression studies using different methods for FACT knockdown (KD) (e.g., SSRP1 short hairpin RNA [shRNA], small interfering RNAs [siRNAs] to SSRP1 and SPT16). We also had nascent RNA-seq data from the same cells (Nesher et al., 2018), which served as a more accurate measure of gene expression, not influenced by the degree of RNA stability. As

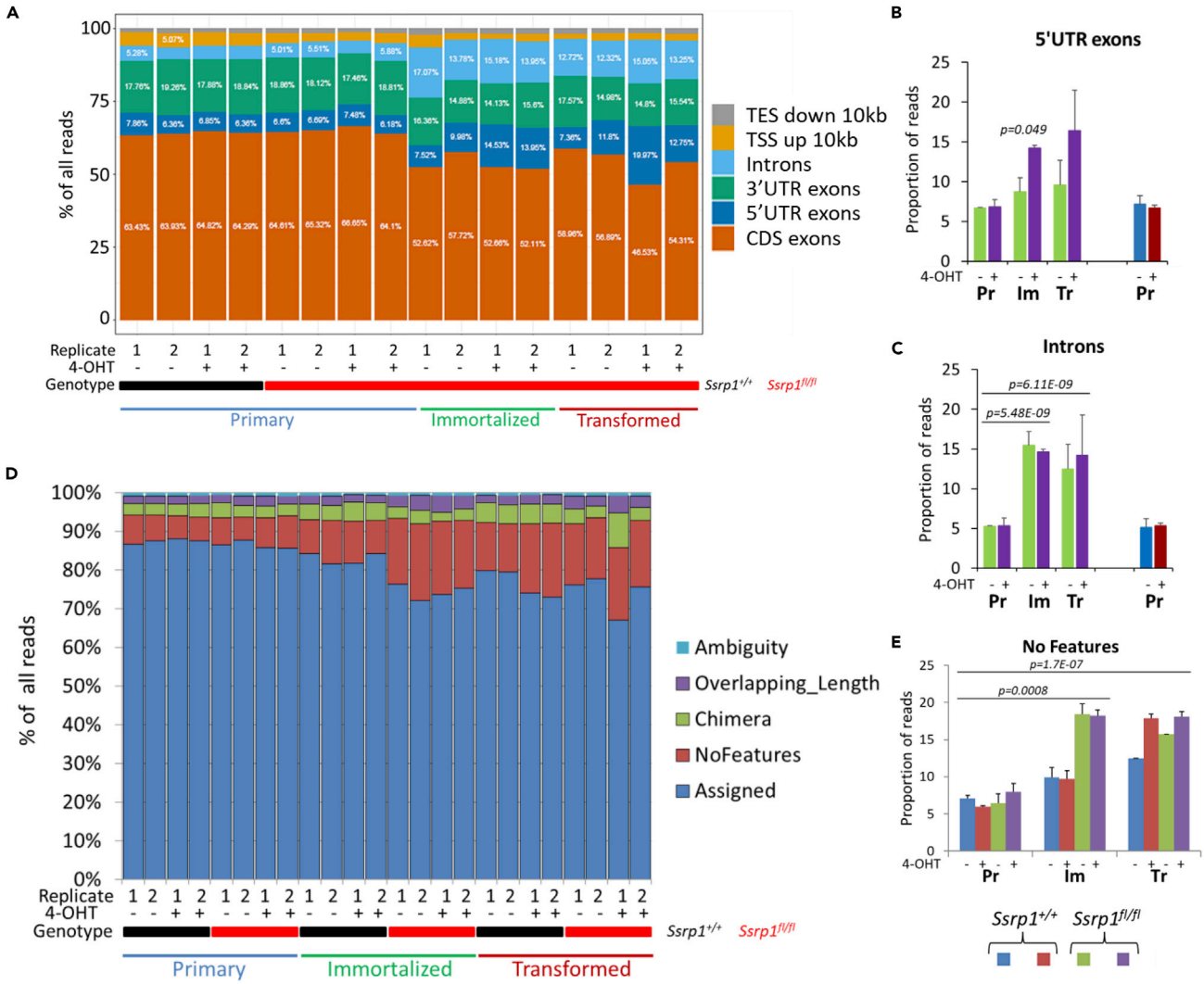

Figure 5. Alterations of Distribution of Transcripts Corresponding to Different Genomic Features upon FACT Loss and Tumorigenic Transformation

(A) Distribution of paired-end RNA-seq reads corresponding to different gene regions within individual samples: TES_down_10kb, read located within 10 kb downstream of the transcription end site; TSS_up_10kb, 10 kb upstream of the transcription start site; introns, within the intron of any gene; 3'UTR_Exons, within the last exon of a gene; 5'UTR_Exon, within the first exon of a gene; CDS_Exons, within all other exons of a gene.

(B and C) Mean proportion of reads corresponding to the first exon (B) or introns (C) within each category of samples ± SD.

(D) Distribution of paired-end RNA-seq reads corresponding to annotated genomic features (Assigned) or not (NoFeatures) as well as reads with questionable annotations (Ambiguity, Chimera, Overlapping_Length) within individual samples.

(E) Mean proportion of reads corresponding to regions with no features within each category of samples ± SD. The same color code is used for (B, C, and E). Similar data for single-end RNA-seq are shown on Figure S10.

we previously observed, there was a significant positive correlation between FACT enrichment and the transcription of genes under basal conditions in these cells (Figure 6A). Interestingly, this dependence was not only quantitative but also qualitative because the profiles of FACT enrichment between 5′ UTR, coding, and 3′ UTR regions were different for genes expressed at different levels (Figure 6B).

Similar to mouse cells, we saw only a negative correlation between FACT enrichment and FACT dependence independent of how expression was measured, i.e., microarray hybridization or RNA sequencing; what approach was used to suppress gene expression (shRNAs or siRNAs to SSRP1, SUPT16H [gene coding SPT16], or both); or whether the correlation analysis was performed using SSRP1 enrichment only at the promoter or coding regions or both (Figures 6C and S11). For the RNA-seq, we used spike-in controls

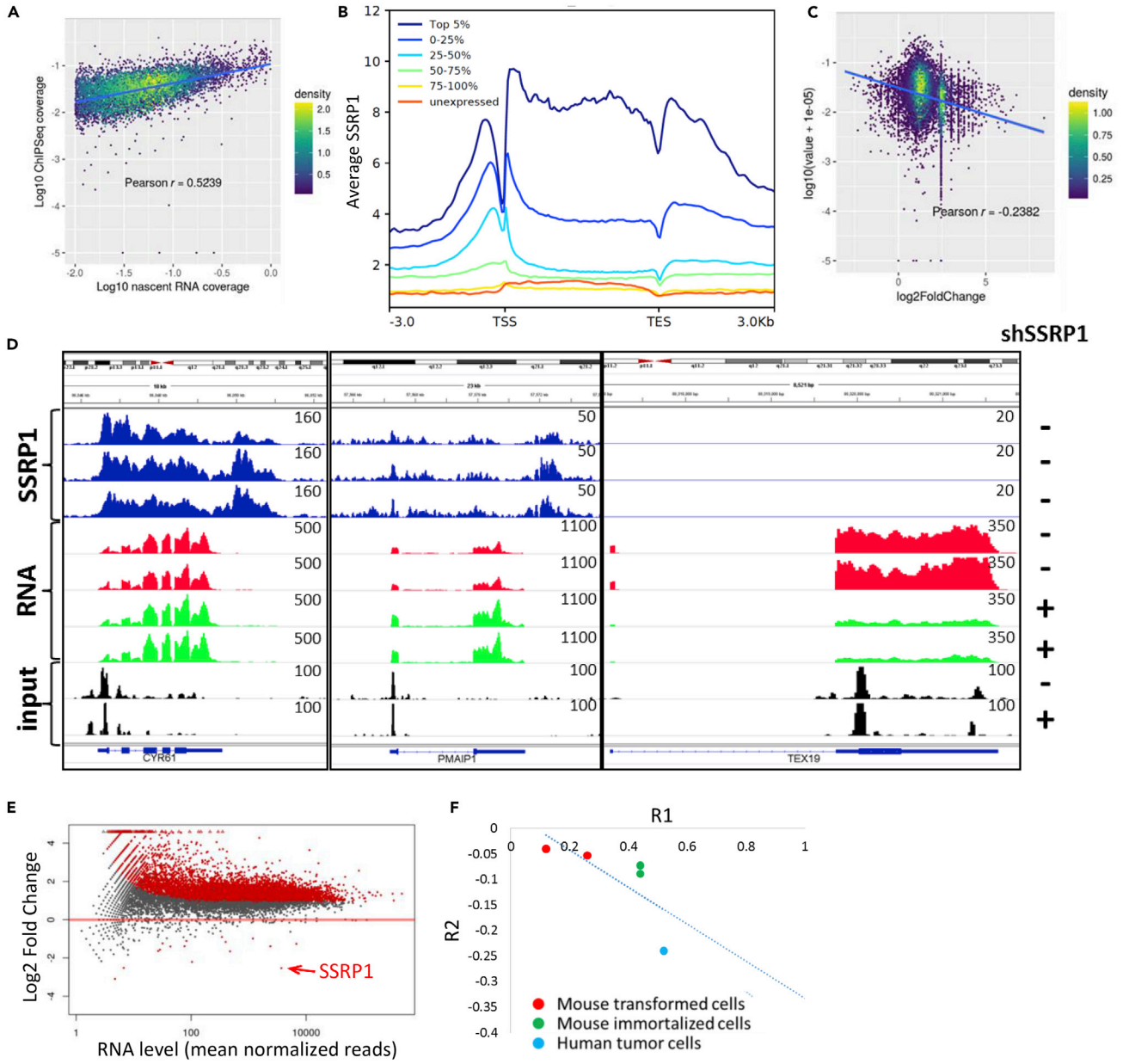

Figure 6. FACT Genomic Distribution and Transcription in Human Cells

(A) Dot plot demonstrating relationship between SSRP1 enrichment (ChIP-seq) and transcription in basal conditions (nascent RNA-seq). R, Pearson correlation coefficient.

(B) Metagene profile of SSRP1 (ChIP-seq) distribution at genes depending on the levels of their transcription defined by nascent RNA-seq read density in basal conditions.

(C) Dot plot demonstrating relationship between SSRP1 enrichment and fold change in gene expression (RNA-seq) upon SSRP1 knockdown with shRNA.

(D) Integrated genomic view of normalized read density of SSRP1 (ChIP-seq, 3 replicates), RNA (RNA-seq, 2 replicates), and input DNA (2 replicates) in cells transduced with control shRNA (–) or shRNA to SSRP1 (+) at three genomic regions surrounding CYR61, PMAIP, and TEX19.

(E) Changes in gene expression between shSSRP1 and shControl cells depending on the level of expression in basal conditions using loess normalized counts. Red dots, fold change > ±1.5, adjusted p value < 0.05.

(F) Inverse relationship between two correlation coefficients, R1, SSRP1 enrichment and gene transcription in basal conditions, and R2, SSRP1 enrichment and FC in gene expression upon FACT depletion, for all tested cells. See also Figure S11.

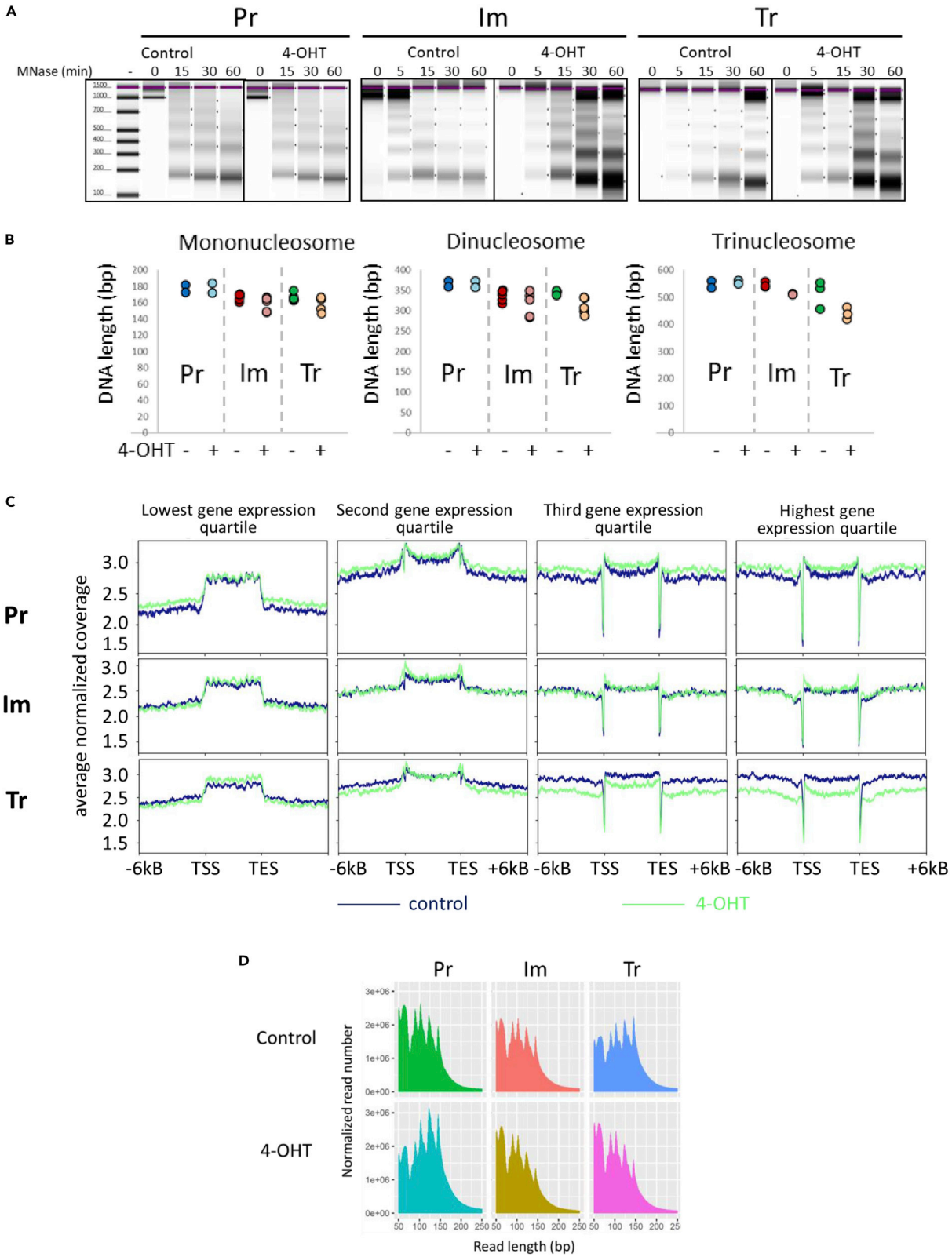
A
Pr
Im
Tr
Control
4-OHT
MNase (min)
B
Mononucleosome
Dinucleosome
Trinucleosome
DNA length (bp)
4-OHT
C
Lowest gene expression quartile
Second gene expression quartile
Third gene expression quartile
Highest gene expression quartile
average normalized coverage
-6kB
TSS
TES
+6kB
control
4-OHT
D
Normalized read number
Read length (bp)

Figure 7. Both FACT Depletion and Tumorigenic Transformation Lead to Chromatin Destabilization

All data are from *Ssrp1*$^{fl/fl}$;*CreERT2*$^{+/+}$ *#2* cells.

(A and B) Sensitivity of chromatin in cells to digestion with micrococci nuclease (MNase) before and after 4-OHT treatment. (A) Images of capillary electrophoresis generated by Bioanalyzer. Images of one representative replicate from Pr, Im, and Tr cells. Images of other replicates are shown in Figure S12. (B) Distribution of length of DNA fragments corresponding to mono-, di-, and tri-nucleosomes obtained upon MNase digestion of chromatin from 4-OHT-treated and control cells detected by Bioanalyzer. Dots are data obtained in several repetitive experiments with cells isolated from different mice.

(C) Metagene profiles of nucleosome distribution obtained by MNase-seq of Pr, Im (#2), and Tr (#2) cells before (blue) and after (green) 4-OHT treatment shown separately for gene expression quartiles (RNA-seq). See also Figures S13 and S14.

(D) Distribution of length of paired-end MNase reads in Pr, Im, and Tr cells with and without 4-OHT treatment.

that allowed us to detect absolute changes in transcription. Consistent with the mouse data, FACT downregulation led to an increase in the transcription of multiple genes. There were more genes enriched for FACT among the upregulated genes than the downregulated genes (Figures 6D and 6E). For the limited number of cases tested, we observed an inverse relationship between the positive correlation coefficient for FACT enrichment at genes versus the transcription in basal conditions and the negative correlation coefficient for FACT enrichment versus the change in expression of genes upon FACT depletion (Figure 6F). These data suggest that the influence of FACT on the transcription of genes is dependent on the type of cell. In general, the stronger was the FACT association with the transcribed genes, the higher was the activation of transcription upon FACT inactivation in cells.

FACT Inactivation Leads to Destabilization of Chromatin in Transformed Cells

Absence of positive effect of FACT on transcription together with the ability of FACT to bind partially unfolded nucleosome and data from lower eukaryotes showing that FACT loss is accompanied by the loss of histones from transcribed regions allows proposing that FACT may help to preserve chromatin at transcribed regions. If this is true in higher eukaryotes, then the loss of FACT should lead to the destabilization of chromatin and suggests a mechanism by which FACT may have negative effect on transcription. If FACT prevents nucleosome loss during transcription, then in the absence of FACT, disassembly of nucleosomes caused by the first RNA polymerase passage should make passage of the next RNA polymerases easier. To test this hypothesis we compared the sensitivity of chromatin to micrococcal nuclease (MNase), which preferentially cleaves protein-free DNA, i.e. leave nucleosomal DNA intact. After 4-OHT treatment of immortalized and transformed cells with *Ssrp1* floxed alleles we observed an increase in the proportion of lower-molecular-weight DNA and a reduction in the length of the DNA fragments protected by the nucleosomes, indicating nucleosome opening (Figures 7A, 7B, and S12). 4-OHT caused no changes in primary cells (Figures 7A, 7B, S12D, and S12E).

Next, we digested chromatin from cells with floxed Ssrp1 to the mononucleosomes using two slightly different regimens of MNase treatment to ensure mononucleosome enrichment in all types of cells and sequenced nucleosome protected fragments (MNase-seq). In general, there was high correlation between these two regimens for all cells (Figures S13 and S14) and the analysis both samples were combined. Figure 7C demonstrates metaplots of nucleosome occupancy in all cell variants with floxed *Ssrp1* before and after 4-OHT treatment. We built these plots separately for each transcription quartile from low to high. First, in all cases there was significant difference in nucleosome occupancy between cells with and without FACT; however, quite surprisingly this difference was opposite between primary and transformed cells, with immortalized being in between. The largest difference was seen at genes with high and moderately high transcription (quartiles 3 and 4): whereas in primary cells nucleosome occupancy was slightly increased, in transformed cells it was substantially decreased upon FACT depletion (Figures 7C and S14). At genes with low and moderate transcription (quartiles 1 and 2) nucleosome occupancy was increased in all types of cells upon FACT removal. Interestingly, nucleosomes were significantly lost before and after coding regions of all genes in transformed cells, but the loss becomes stronger with an increase of gene transcription.

Decrease in nucleosome-protected DNA fragments (135–200 bp length) may be the result of reduced number of nucleosomes (e.g., random loss of nucleosomes or increase in linker DNA length) or presence of nucleosomes in more open state, such as nucleosomes without linker histones or without one H2A/B dimer (subnucleosomal particles) (Tsunaka et al., 2016; Safina et al., 2017; Wang et al., 2018a; Liu et al., 2020). To test this we compared distribution of paired-end read length in MNase data. We have found that after

4-OHT treatment there was significant decrease in 147-bp fragment size in transformed cells, slight decrease in immortalized cells, and increase in primary cells (Figure 7D). Concomitantly, there were more short fragments in transformed and to a lesser extent in immortalized cells and less short fragments in primary cells.

Thus, we observed that depletion of FACT has almost different consequences for normal and transformed cells. Normal cells without FACT have nucleosomes as or even more "stable" than normal cells with FACT: average nucleosome occupancy is increased with higher proportion of longer nucleosome-protected DNA fragments, and nucleosome dynamics are not visibly changed. Stability of nucleosomes in transformed cells without FACT is significantly decreased; there is lower nucleosome occupancy and higher proportion of shorter DNA fragments suggesting the presence of more open nucleosomes or subnucleosomal particles.

DISCUSSION

The goal of our study was to understand why malignant tumor cells are much more dependent on FACT than less malignant and non-tumor cells. FACT function established in cell-free experiments as facilitation of RNA polymerase passage through nucleosomes makes difficult to explain differential cell dependence on FACT, because nucleosomes are present at coding regions of all genes in all mammalian cells. Thus, we designed this study to compare consequences of FACT loss in original FACT-independent cells and cells that we made dependent on FACT via established genetic manipulations, i.e., inactivation of tumor suppressor p53 and overexpression of mutant $HRas^{V12}$ oncogene. These cells as expected became fully transformed, i.e., anchorage independent and forming aggressive tumors in mice, thus representing a model of malignant tumor cells.

Our initial hypothesis was that FACT is needed not for all transcription elongation, but for the most efficient high-rate transcription. In support of this hypothesis, we and others observed correlation between FACT enrichment genome-wide and rates of transcription (Mylonas and Tessarz, 2018; Kolundzic et al., 2018; Heo et al., 2008). However, inactivation of FACT did not reduce the rates of transcription in any of the tested cells, ruling out the proposition that FACT is needed for transcription elongation.

Although there were some genes with reduced expression following loss of FACT, coding regions of these genes were not enriched with FACT under basal conditions. Moreover, there was a negative correlation between FACT enrichment and changes in gene transcription, suggesting that FACT inhibits transcription of genes.

Thus, FACT enrichment genome-wide depends on transcription, but transcription does not depend on FACT, suggesting that FACT does not facilitate transcription elongation. Indeed, our studies and the existing FACT literature suggest that instead of disassembly, FACT preserves the nucleosomes that are disturbed by the passage of the RNA polymerase (Gurova et al., 2018). If RNA polymerase itself or together with other factors destabilizes nucleosomes, the stabilization or reassembly of nucleosomes by FACT will prevent the loss of histones. Furthermore, the model explains why FACT is enriched in proportion to the level of transcription. The more frequently RNA polymerases pass through a gene, the more often nucleosomes are disturbed, increasing the chance of FACT binding.

Our current model of FACT function is consistent with published structural studies that showed that mammalian FACT could only bind nucleosomal components or subnucleosomal particles (e.g., lacking the H2A/H2B dimer) because the FACT-binding epitopes are hidden within the folded nucleosome (Safina et al., 2017; Tsunaka et al., 2016; Wang et al., 2018). It is also consistent with studies in yeast that showed that FACT is targeted to transcribed chromatin through its recognition of RNA polymerase-disrupted nucleosomes (Martin et al., 2018) and the loss of FACT is accompanied by the loss of histones and pervasive transcription (Erkina and Erkine, 2015; Feng et al., 2016; Morillo-Huesca et al., 2010; Myers et al., 2011). Similar observations in plants have also been recently reported (Nielsen et al., 2019).

If the above model is correct, why is transcription increased following the loss of FACT? There are two potential explanations for this phenomenon, which will require further investigation. First, in the absence of FACT, nucleosomes that are destabilized by the first RNA polymerase passage will be a weaker barrier for subsequent passages by RNA polymerases. Thus, gene transcription will become more efficient.

Alternatively, or in addition, nucleosomes may eventually be lost from the transcribed regions, leading to cryptic initiation and pervasive transcription. With short read-based transcription analysis, it is difficult to distinguish between these two scenarios. We expected that cryptic initiation and pervasive transcription would skew the distribution of RNA-seq reads corresponding to the 5′ and -3′ exons of the genes. In line with this we observed higher proportion of reads corresponding to 5′ exons in transformed and immortalized cells upon FACT depletion using RNA-seq.

The most interesting question is why FACT loss is only problematic for transformed and tumor cells if it serves a very basic function of prevention of the loss of histones from destabilized nucleosomes during transcription and replication. Although both processes occur in primary cells, FACT loss is not associated with reduced viability of these cells and destabilization of chromatin. One explanation is that replication and transcription occur at a lower rate in the primary cells than in the immortalized and transformed cells, and therefore the rate of these processes could be one factor that determined the necessity of FACT. However, this hypothesis was disproven by a recent report that demonstrated increased proliferation of mouse embryonic stem cells, which typically have very high replication and transcription rates (Efroni et al., 2008), upon FACT KD (Mylonas and Tessarz, 2018).

Another hypothesis of why FACT is essential for transformed and tumor cells is that it is needed for the packaging of DNA for mitosis, which is a constantly ongoing process in these cells. FACT was found to be one of only a few factors that were essential for packaging mitotic chromosomes under cell-free conditions (Shintomi et al., 2015). However, the ability of primary and other non-tumor cells to pass through mitosis in the absence of FACT shakes this proposition.

The third hypothesis is that FACT prevents nucleosome loss in transformed and tumor cells, in which chromatin is already destabilized compared with non-tumor cells and therefore two chromatin-destabilizing effects, transformation and FACT loss, together drive chromatin state to the critical lethal point. We showed that both transformation and FACT loss reduced nucleosome stability. Nucleosome stability is a well-defined property of nucleosomes in cell-free experiments, which can be measured by different methods, including resistance to increased concentrations of salt and protection of nucleosomal DNA from nuclease digestion. However, in mammalian cells, there are millions of nucleosomes, and their stability differs significantly at different genomic loci and depends on a large number of factors. Therefore, understanding nucleosome stability in the context of cells is more difficult. To make this concept easier, we propose to define nucleosome stability in cells as a degree of this nucleosome interference with transcription. In general, regions of constitutive heterochromatin in mammalian cells have more stable nucleosomes (Riedmann and Fondufe-Mittendorf, 2016; Collings et al., 2013), whereas nucleosomes in transcribed regions are less stable and more open (Brower-Toland et al., 2005). Nucleosomes at AT-rich DNA (e.g., promoters and TSS regions) are also less stable (Lorch et al., 2014).

Based on indirect literature data and observations made in the current study, we propose that, in general, chromatin is destabilized upon malignant transformation. It becomes more sensitive to nucleases, has a higher histone exchange rate, and is less restrictive to transcription (judged by the appearance of reads with no features and corresponding to introns). Data available in the literature suggest that changes in the chromatin state may be a universal process that accompanies malignant transformation. Reports have shown that tumors can have reduced expression of linker histone 1 (Scaffidi, 2016), their DNA is hypomethylated (Ehrlich, 2009). Tumor cells have reduced amount of architectural chromatin proteins (e.g., HP1) that could make chromatin less stable (Dialynas et al., 2008), and increased levels of HMG box proteins, which can unwrap DNA from nucleosomes at entry and exit points (Hock et al., 2007). In addition, we observed a higher sensitivity of tumor cells to chromatin-destabilizing small molecules, which suggests that chromatin in tumor cells may be less stable under basal conditions than in normal cells (Gasparian et al., 2011; Safina et al., 2017).

We observed an interesting relationship between FACT and transcription in immortalized and transformed cells, which was different from that observed in normal mammalian stem and non-stem cells (Mylonas and Tessarz, 2018; Kolundzic et al., 2018). In immortalized cells, FACT enrichment was more proportional to the level of gene transcription than that observed in transformed cells. When FACT was depleted from the immortalized cells, there was a higher increase in transcription of the FACT-enriched genes compared with the transformed cells. Based on these data, the ability of FACT to rebuild nucleosomes at transcribed genes may be stronger in immortalized cells than in transformed cells. In transformed cells, the levels of

FACT and FACT enrichment at non-transcribed genes and non-genic regions are higher. Because chromatin is less stable in transformed cells, there is broader pervasive transcription. Thus, FACT function is needed not only at transcribed genes, but genome-wide, which results in smudging of FACT profiles between gene and non-gene regions.

On the background of already destabilized chromatin, the loss of FACT further destabilizes chromatin as judged by the reduction of nucleosome occupancy and shift in the ratio of DNA fragments from longer to shorter. This is partially observed in cells lacking p53, but not in primary cells. In opposite, it looks like loss of FACT makes nucleosomes even more stable, because we observed increased nucleosome occupancy and DNA fragment size in these cells. However, we were not able to detect functional consequences of these changes in primary cells.

Taken together, our findings suggest that FACT is essential for tumor cells to compensate for the general destabilization of chromatin, which cells acquire during the process of transformation. Therefore, the level of FACT in cells may be considered as a measure or marker of chromatin instability in mammalian cells.

Limitations of the Study

First, we cannot exclude that the absence of FACT in normal cells is compensated by another factor, which prevents nucleosome loss from chromatin during transcription. However, the data showing increase in nucleosome occupancy in normal cells after removal of FACT suggest that most probably either nucleosome organization or FACT function is different between normal and tumor cells. This will require further investigation. Proposed reason of FACT dependency as the presence of less stable chromatin in tumor cells needs to be tested in human tumors, although direct comparison is difficult in this case, because human cells of origin of many cancer types are still unknown. We also do not know what makes chromatin less stable in tumors, and whether this is a cause or consequence of malignant transformation. Currently, we also know very little about the consequences of chromatin destabilization in cells. We recently proposed several mechanisms (Gurova, 2019), but they have not been explored experimentally. An additional intriguing and unresolved question is why FACT loss makes nucleosomes less stable in transformed cells, whereas more stable in primary cells.

Resource Availability

Lead Contact

Katerina Gurova, Department of Cell Stress Biology, Roswell Park Comprehensive Cancer Center, Carlton and Elm Streets, Buffalo, NY, 14127; tel: 1-716-845-4760, fax: 1-716-845-3944, email: katerina.gurova@roswellpark.org.

Material Availability

All materials from this study are available upon request.

Data and Code Availability

All NGS data were submitted to GEO database. Mouse RNA-sequencing data are available as GSE132695, mouse MNase-seq data are available as GSE149951, HT1080 human fibrosarcoma cell data nascent RNA-seq as GSE107633, and SSRP1 ChIP-seq as GSE107595 and GSE45393.

METHODS

All methods can be found in the accompanying Transparent Methods supplemental file.

SUPPLEMENTAL INFORMATION

Supplemental Information can be found online at https://doi.org/10.1016/j.isci.2020.101177.

ACKNOWLEDGMENTS

We are grateful to Prashant Singh from Genomics Shared Resource of Roswell Park Comprehensive Cancer for being always available to help with processing of our sequenceing needs, to Caterine Burkhart from Burkhart Documents Solutions for critical reading and editing of the manuscript.

Funding: National Cancer Institute: R01CA197967: Katerina V. Gurova; National Cancer Institute: R21CA198395: K.V.G.; National Cancer Institute: P30CA016056: to Roswell Park Comprehensive Cancer Center; Susan G. Komen (US): CCR13264604: K.V.G.; Incuron LLC: K.V.G.

AUTHOR CONTRIBUTIONS

P.S., design and execution of most of experiments and writing and editing of the manuscript; A.S., preparation of samples for ChIP-sequencing and MNase-seq; I.G., isolation of cells from animals and MNAse digestion experiments; L.P., analysis of DNA damage in cells; S.R., analysis of RNA-seq data; E.C.G., analysis of RNA-seq data; J.W., all bioinformatics processing and analyses; K.V.G., development of the concept of the study, design and analyses of data, writing and editing of the manuscript.

DECLARATION OF INTERESTS

Authors declare no competing interests.

Received: May 8, 2019
Revised: March 23, 2020
Accepted: May 14, 2020
Published: June 26, 2020

REFERENCES

Attwood, K., Fleyshman, D., Prendergast, L., Paszkiewicz, G., Omilian, A.R., Bshara, W., and Gurova, K. (2017). Prognostic value of histone chaperone FACT subunits expression in breast cancer. Breast Cancer (Dove Med. Press) *9*, 301–311.

Brower-Toland, B., Wacker, D.A., Fulbright, R.M., Lis, J.T., Kraus, W.L., and Wang, M.D. (2005). Specific contributions of histone tails and their acetylation to the mechanical stability of nucleosomes. J. Mol. Biol. *346*, 135–146.

Cao, S., Bendall, H., Hicks, G.G., Nashabi, A., Sakano, H., Shinkai, Y., Gariglio, M., Oltz, E.M., and Ruley, H.E. (2003). The high-mobility-group box protein SSRP1/T160 is essential for cell viability in day 3.5 mouse embryos. Mol. Cell. Biol. *23*, 5301–5307.

Carter, D.R., Murray, J., Cheung, B.B., Gamble, L., Koach, J., Tsang, J., Sutton, S., Kalla, H., Syed, S., Gifford, A.J., et al. (2015). Therapeutic targeting of the MYC signal by inhibition of histone chaperone FACT in neuroblastoma. Sci. Transl. Med. *7*, 312ra176.

Carvalho, S., Raposo, A.C., Martins, F.B., Grosso, A.R., Sridhara, S.C., Rino, J., Carmo-Fonseca, M., and de Almeida, S.F. (2013). Histone methyltransferase SETD2 coordinates FACT recruitment with nucleosome dynamics during transcription. Nucleic Acids Res. *41*, 2881–2893.

Collings, C.K., Waddell, P.J., and Anderson, J.N. (2013). Effects of DNA methylation on nucleosome stability. Nucleic Acids Res. *41*, 2918–2931.

Dermawan, J.K., Hitomi, M., Silver, D.J., Wu, Q., Sandlesh, P., Sloan, A.E., Purmal, A.A., Gurova, K.V., Rich, J.N., Lathia, J.D., et al. (2016). Pharmacological targeting of the histone chaperone complex FACT preferentially eliminates glioblastoma stem cells and prolongs survival in preclinical models. Cancer Res. *76*, 2432–2442.

Dialynas, G.K., Vitalini, M.W., and Wallrath, L.L. (2008). Linking heterochromatin protein 1 (HP1) to cancer progression. Mutat. Res. *647*, 13–20.

Ding, Q., He, K., Luo, T., Deng, Y., Wang, H., Liu, H., Zhang, J., Chen, K., Xiao, J., Duan, X., et al. (2016). SSRP1 contributes to the malignancy of hepatocellular carcinoma and is negatively regulated by miR-497. Mol. Ther. *24*, 903–914.

Dvinge, H., and Bradley, R.K. (2015). Widespread intron retention diversifies most cancer transcriptomes. Genome Med. *7*, 45.

Efroni, S., Duttagupta, R., Cheng, J., Dehghani, H., Hoeppner, D.J., Dash, C., Bazett-Jones, D.P., Le Grice, S., McKay, R.D., Buetow, K.H., et al. (2008). Global transcription in pluripotent embryonic stem cells. Cell Stem Cell *2*, 437–447.

Ehrlich, M. (2009). DNA hypomethylation in cancer cells. Epigenomics *1*, 239–259.

Erkina, T.Y., and Erkine, A. (2015). ASF1 and the SWI/SNF complex interact functionally during nucleosome displacement, while FACT is required for nucleosome reassembly at yeast heat shock gene promoters during sustained stress. Cell Stress Chaperones *20*, 355–369.

Feng, J., Gan, H., Eaton, M.L., Zhou, H., Li, S., Belsky, J.A., MacAlpine, D.M., Zhang, Z., and Li, Q. (2016). Noncoding transcription is a driving force for nucleosome instability in spt16 mutant cells. Mol. Cell. Biol. *36*, 1856–1867.

Ferraro, A. (2016). Altered primary chromatin structures and their implications in cancer development. Cell Oncol. (Dordr.) *39*, 195–210.

Flavahan, W.A., Gaskell, E., and Bernstein, B.E. (2017). Epigenetic plasticity and the hallmarks of cancer. Science *357*, https://doi.org/10.1126/science.aal2380.

Fleyshman, D., Prendergast, L., Safina, A., Paszkiewicz, G., Commane, M., Morgan, K., Attwood, K., and Gurova, K. (2017). Level of FACT defines the transcriptional landscape and aggressive phenotype of breast cancer cells. Oncotarget *8*, 20525–20542.

Fragkos, M., and Naim, V. (2017). Rescue from replication stress during mitosis. Cell Cycle *16*, 613–633.

Garcia, H., Fleyshman, D., Kolesnikova, K., Safina, A., Commane, M., Paszkiewicz, G., Omelian, A., Morrison, C., and Gurova, K. (2011). Expression of FACT in mammalian tissues suggests its role in maintaining of undifferentiated state of cells. Oncotarget *2*, 783–796.

Garcia, H., Miecznikowski, J.C., Safina, A., Commane, M., Ruusulehto, A., Kilpinen, S., Leach, R.W., Attwood, K., Li, Y., Degan, S., et al. (2013). Facilitates chromatin transcription complex is an "accelerator" of tumor transformation and potential marker and target of aggressive cancers. Cell Rep. *4*, 159–173.

Gasparian, A.V., Burkhart, C.A., Purmal, A.A., Brodsky, L., Pal, M., Saranadasa, M., Bosykh, D.A., Commane, M., Guryanova, O.A., Pal, S., et al. (2011). Curaxins: anticancer compounds that simultaneously suppress NF-kappaB and activate p53 by targeting FACT. Sci. Transl. Med. *3*, 95ra74.

Gurova, K.V. (2019). Chromatin stability as a target for cancer treatment. Bioessays *41*, e1800141.

Gurova, K., Chang, H.W., Valieva, M.E., Sandlesh, P., and Studitsky, V.M. (2018). Structure and function of the histone chaperone FACT - resolving FACTual issues. Biochim. Biophys. Acta Gene Regul. Mech. *1861*, 892–904.

Heo, K., Kim, H., Choi, S.H., Choi, J., Kim, K., Gu, J., Lieber, M.R., Yang, A.S., and An, W. (2008). FACT-mediated exchange of histone variant H2AX regulated by phosphorylation of H2AX and ADP-ribosylation of Spt16. Mol. Cell *30*, 86–97.

Hock, R., Furusawa, T., Ueda, T., and Bustin, M. (2007). HMG chromosomal proteins in

development and disease. Trends Cell Biol. *17*, 72–79.

Hsieh, F.K., Kulaeva, O.I., Patel, S.S., Dyer, P.N., Luger, K., Reinberg, D., and Studitsky, V.M. (2013). Histone chaperone FACT action during transcription through chromatin by RNA polymerase II. Proc. Natl. Acad. Sci. U S A *110*, 7654–7659.

Kolundzic, E., Ofenbauer, A., Bulut, S.I., Uyar, B., Baytek, G., Sommermeier, A., Seelk, S., He, M., Hirsekorn, A., Vucicevic, D., et al. (2018). FACT sets a barrier for cell fate reprogramming in Caenorhabditis elegans and human cells. Dev. Cell *46*, 611–626 e12.

Liu, Y., Zhou, K., Zhang, N., Wei, H., Tan, Y.Z., Zhang, Z., Carragher, B., Potter, C.S., D'Arcy, S., and Luger, K. (2020). FACT caught in the act of manipulating the nucleosome. Nature *577*, 426–431.

Loonstra, A., Vooijs, M., Beverloo, H.B., Allak, B.A., van Drunen, E., Kanaar, R., Berns, A., and Jonkers, J. (2001). Growth inhibition and DNA damage induced by Cre recombinase in mammalian cells. Proc. Natl. Acad. Sci. U S A *98*, 9209–9214.

Lorch, Y., Maier-Davis, B., and Kornberg, R.D. (2014). Role of DNA sequence in chromatin remodeling and the formation of nucleosome-free regions. Genes Dev. *28*, 2492–2497.

Martin, B.J.E., Chruscicki, A.T., and Howe, L.J. (2018). Transcription promotes the interaction of the FAcilitates chromatin transactions (FACT) complex with nucleosomes in Saccharomyces cerevisiae. Genetics *210*, 869–881.

Morgan, M.A., and Shilatifard, A. (2015). Chromatin signatures of cancer. Genes Dev. *29*, 238–249.

Morillo-Huesca, M., Maya, D., Munoz-Centeno, M.C., Singh, R.K., Oreal, V., Reddy, G.U., Liang, D., Geli, V., Gunjan, A., and Chavez, S. (2010). FACT prevents the accumulation of free histones evicted from transcribed chromatin and a subsequent cell cycle delay in G1. PLoS Genet. *6*, e1000964.

Myers, C.N., Berner, G.B., Holthoff, J.H., Martinez-Fonts, K., Harper, J.A., Alford, S., Taylor, M.N., and Duina, A.A. (2011). Mutant versions of the S. cerevisiae transcription elongation factor Spt16 define regions of Spt16 that functionally interact with histone H3. PLoS One *6*, e20847.

Mylonas, C., and Tessarz, P. (2018). Transcriptional repression by FACT is linked to regulation of chromatin accessibility at the promoter of ES cells. Life Sci. Alliance *1*, e201800085.

Nesher, E., Safina, A., Aljahdali, I., Portwood, S., Wang, E.S., Koman, I., Wang, J., and Gurova, K.V. (2018). Role of chromatin damage and chromatin trapping of FACT in mediating the anticancer cytotoxicity of DNA-binding small-molecule drugs. Cancer Res. *78*, 1431–1443.

Nielsen, M., Ard, R., Leng, X., Ivanov, M., Kindgren, P., Pelechano, V., and Marquardt, S. (2019). Transcription-driven chromatin repression of Intragenic transcription start sites. PLoS Genet. *15*, e1007969.

Orphanides, G., Leroy, G., Chang, C.H., Luse, D.S., and Reinberg, D. (1998). FACT, a factor that facilitates transcript elongation through nucleosomes. Cell *92*, 105–116.

Orphanides, G., Wu, W.H., Lane, W.S., Hampsey, M., and Reinberg, D. (1999). The chromatin-specific transcription elongation factor FACT comprises human SPT16 and SSRP1 proteins. Nature *400*, 284–288.

Ossovskaya, V.S., Mazo, I.A., Chernov, M.V., Chernova, O.B., Strezoska, Z., Kondratov, R., Stark, G.R., Chumakov, P.M., and Gudkov, A.V. (1996). Use of genetic suppressor elements to dissect distinct biological effects of separate p53 domains. Proc. Natl. Acad. Sci. U S A *93*, 10309–10314.

Riedmann, C., and Fondufe-Mittendorf, Y.N. (2016). Comparative analysis of linker histone H1, MeCP2, and HMGD1 on nucleosome stability and target site accessibility. Sci. Rep. *6*, 33186.

Safina, A., Cheney, P., Pal, M., Brodsky, L., Ivanov, A., Kirsanov, K., Lesovaya, E., Naberezhnov, D., Nesher, E., Koman, I., et al. (2017). FACT is a sensor of DNA torsional stress in eukaryotic cells. Nucleic Acids Res. *45*, 1925–1945.

Safina, A., Garcia, H., Commane, M., Guryanova, O., Degan, S., Kolesnikova, K., and Gurova, K.V. (2013). Complex mutual regulation of facilitates chromatin transcription (FACT) subunits on both mRNA and protein levels in human cells. Cell Cycle *12*, 2423–2434.

Sandlesh, P., Juang, T., Safina, A., Higgins, M.J., and Gurova, K.V. (2018). Uncovering the fine print of the CreERT2-LoxP system while generating a conditional knockout mouse model of Ssrp1 gene. PLoS One *13*, e0199785.

Scaffidi, P. (2016). Histone H1 alterations in cancer. Biochim. Biophys. Acta *1859*, 533–539.

Shintomi, K., Takahashi, T.S., and Hirano, T. (2015). Reconstitution of mitotic chromatids with a minimum set of purified factors. Nat. Cell Biol. *17*, 1014–1023.

Smart, A.C., Margolis, C.A., Pimentel, H., He, M.X., Miao, D., Adeegbe, D., Fugmann, T., Wong, K.K., and van Allen, E.M. (2018). Intron retention is a source of neoepitopes in cancer. Nat. Biotechnol. *36*, 1056–1058.

Tsunaka, Y., Fujiwara, Y., Oyama, T., Hirose, S., and Morikawa, K. (2016). Integrated molecular mechanism directing nucleosome reorganization by human FACT. Genes Dev. *30*, 673–686.

Wang, T., Liu, Y., Edwards, G., Krzizike, D., Scherman, H., and Luger, K. (2018). The histone chaperone FACT modulates nucleosome structure by tethering its components. Life Sci. Alliance *1*, e201800107.

Wong, J.J., Au, A.Y., Ritchie, W., and Rasko, J.E. (2016). Intron retention in mRNA: No longer nonsense: known and putative roles of intron retention in normal and disease biology. Bioessays *38*, 41–49.

iScience, Volume *23*

Supplemental Information

Prevention of Chromatin Destabilization by FACT Is Crucial for Malignant Transformation

Poorva Sandlesh, Alfiya Safina, Imon Goswami, Laura Prendergust, Spenser Rosario, Eduardo C. Gomez, Jianmin Wang, and Katerina V. Gurova

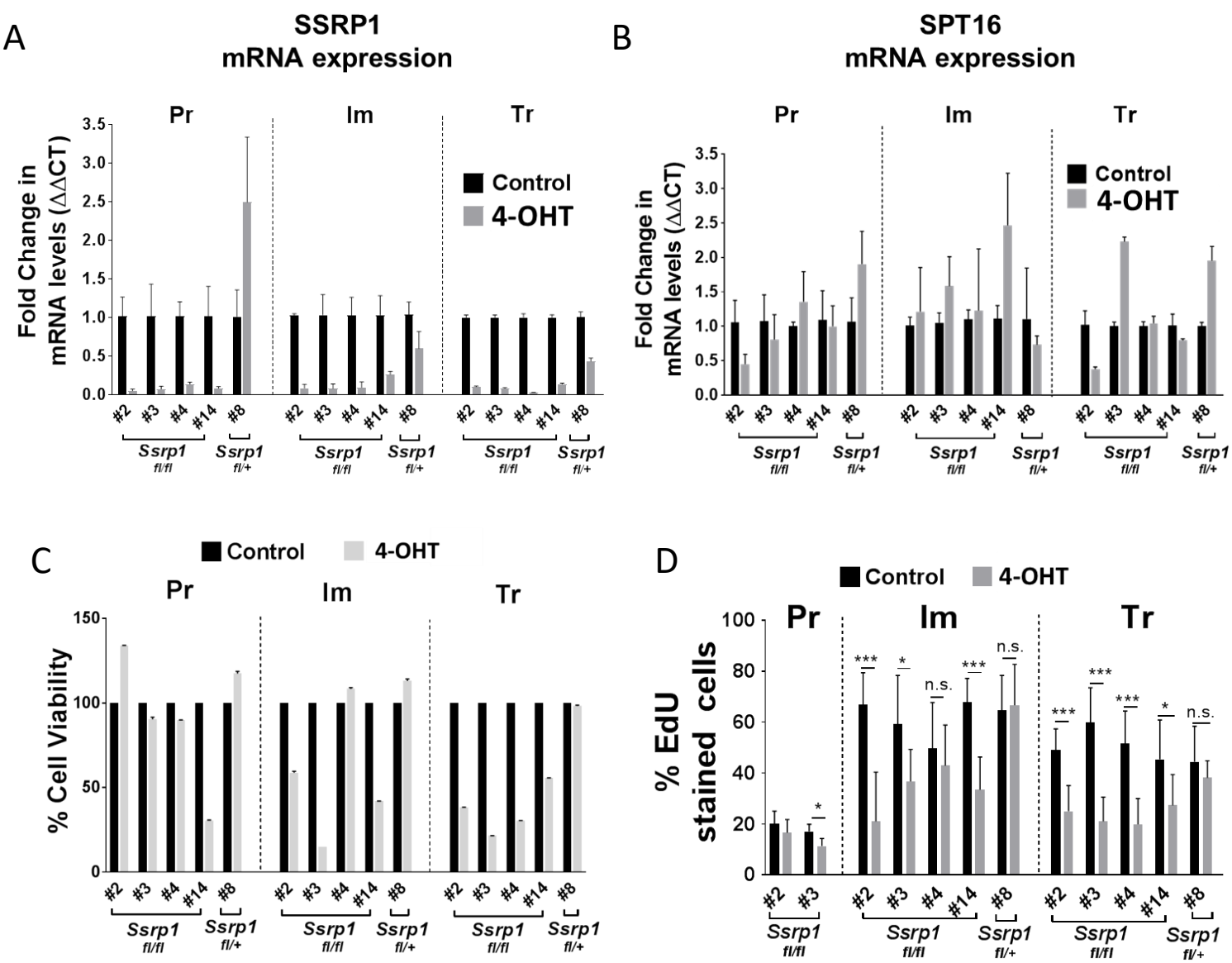

Figure S1 related to Figure 2. Effect of 4-OHT administration on primary (Pr), immortalized (Im) and transformed (Tr) cells established from *Ssrp1$^{fl/fl}$;CreER$^{T2+/+}$ or Ssrp1$^{fl/+}$;CreER$^{T2+/+}$* mice. A, B. mRNA levels of *Ssrp1* (A) and *Supt16* (gene encoding SPT16) (B) in Pr, Im and Tr MSFs from *Ssrp1$^{fl/fl}$ CreER$^{T2+/+}$* (#2, #3, #4, #14) and *Ssrp1$^{fl/+}$ CreER$^{T2+/+}$* (#8) mice. The expression levels were measured using qRT-PCR and are presented relative to the untreated cells. Data are presented as the mean ± SD (n = 3). C. Viability of Pr, Im and Tr MSFs with and without 4-OHT treatment. Data are presented as the mean ± SD (n = 3). D. EdU incorporation assay. P-values * <0.01, **<0.001 and ***<0.0001.

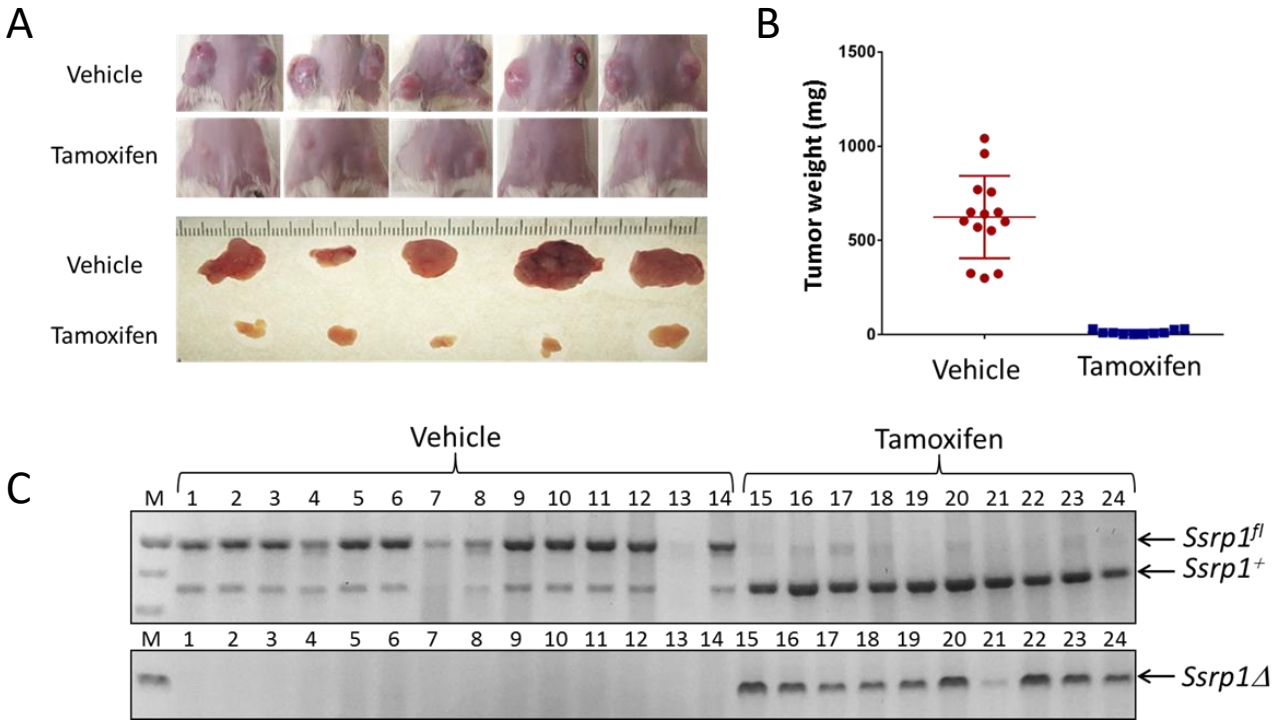

Figure S2 related to Figure 2. **Effect of tamoxifen administration of the growth of transformed cells in SCID mice**. A. Photographs of mice and tumors at the end of experiment (day 32). B. Weight of tumors at the end of experiment. C. Testing of excision of *Ssrp1* (appearance of *Ssrp1Δ*) in tumors at the end of treatment with tamoxifen using PCR of genomic DNA extracted from individual tumors. $Ssrp1^{fl}$ - mutant allele. $Ssrp1^{+}$ - wild type *Ssrp1* and *Ssrp1Δ* - excised allele. Wild type *Ssrp1* ($Ssrp1^{+}$) is present in tamoxifen treated tumors most probably due to the presence of stroma.

A

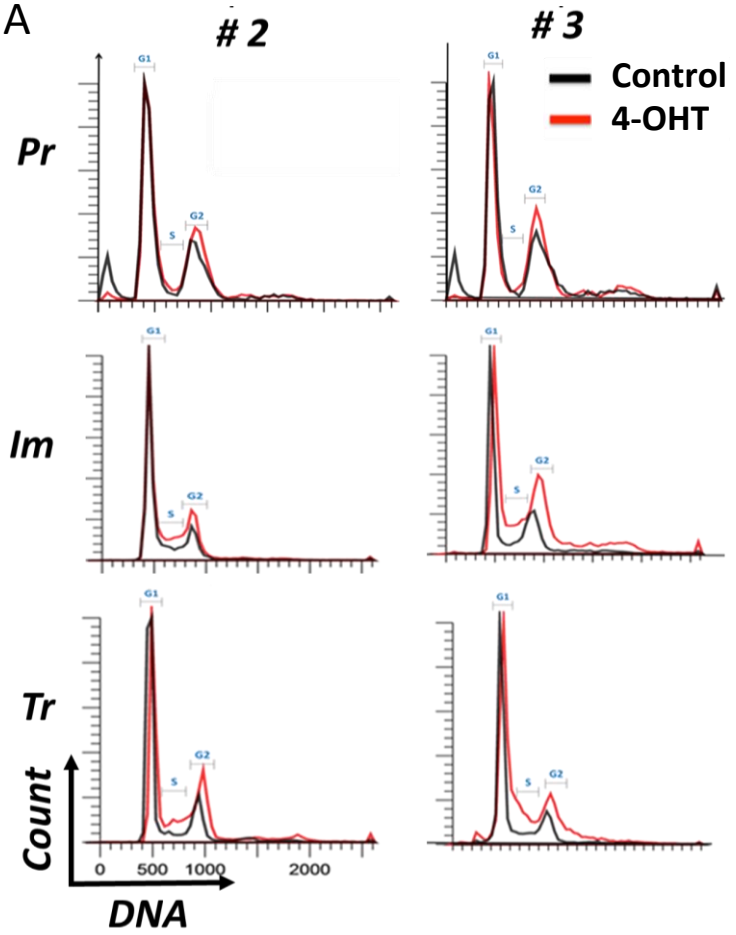

B

Genotype	Phenotype		G0		G1		S		G2/M	
		Cell #	Control	+ 4OHT (2μM)	Control	+ 4OHT (2μM)	Control	+ 4OHT (2μM)	Control	+ 4OHT (2μM)
Ssrp1$^{fl/fl}$ *CreER*$^{T2+/+}$	Primary	#2	5.57	0.82	51.28	44.39	2.35	3.32	27.92	32.27
		#3	7.92	1.08	45.92	41.85	2.37	5.36	26.16	33.54
	Immortalized	#2	0.01	0.05	62.61	51.34	10.33	15.57	22.64	37.85
		#3	0.07	0.33	54.04	29.02	7.64	15.64	25.45	37.12
	Transformed	#2	0.03	0.14	68.23	45.04	10.17	22.52	17.79	29.12
		#3	0.19	0.66	59.68	42.13	12.78	24.91	20.78	35.13
Ssrp1$^{fl/+}$ *CreER*$^{T2+/+}$	Immortalized	#8	0.07	0.23	44.27	46.86	21.92	20.02	28.56	28.8
	Transformed	#8	0.11	0.14	59.44	56.33	12.98	13.34	13.4	15.09

C

		Aver		T test	SDV	
		Control	+ 4OHT (2μM)		Control	+ 4OHT (2μM)
G1	Primary	48.6	43.12	0.080162	2.68	1.27
	Immortalized	58.325	40.18	0.115285	4.285	11.16
	Transformed	63.955	43.585	0.043788	4.275	1.455
S	Primary	2.36	4.34	0.150145	0.01	1.02
	Immortalized	8.985	15.605	0.065418	1.345	0.035
	Transformed	11.475	23.715	0.002861	1.305	1.195
G2/M	Primary	27.04	32.905	0.080464	0.88	0.635
	Immortalized	24.045	37.485	0.04168	1.405	0.365
	Transformed	19.285	32.125	0.037262	1.495	3.005

Figure S3 related to Figure 2. Effect of *Ssrp1* KO on the cell cycle distribution in primary (Pr), immortalized (Im), and transformed (Tr) cells. A. Cell cycle distribution profiles for *Ssrp1*$^{fl/fl}$ *CreER*$^{T2+/+}$ cells treated with 4-OHT (red) or vehicle (black). B. Quantitation of cell cycle distribution data using ModFit. C. Statistical evaluation of the cell cycle distribution data.

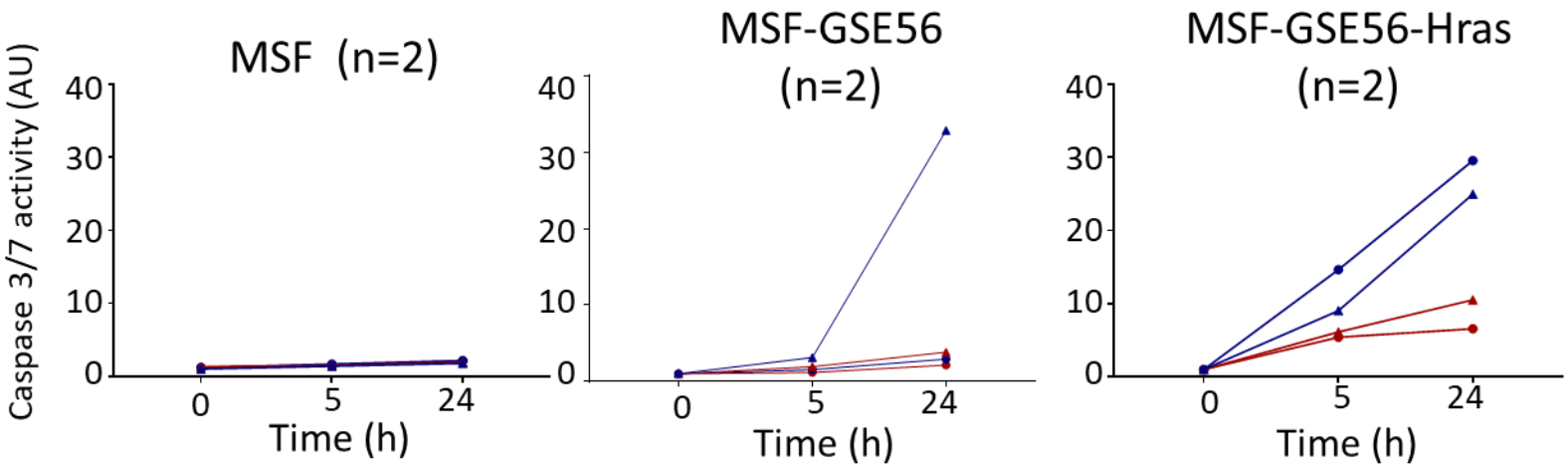

Figure S4 related to Figure 2. Effect of *Ssrp1* KO on the activity of caspases in primary (MSF), immortalized (MSF-GSE56), and transformed (MSF-GSE56-Hras) cells. A. *Ssrp1*$^{fl/fl}$ *CreER*$^{T2+/+}$ cells were treated with 4-OHT (red) or vehicle (blue) for 5 days, then replated and caspase3/7 substrate was added to cell culture lysates for the indicated amount of time. All readings were normalized by the readings obtained immediately after substrate addition (0 hours).

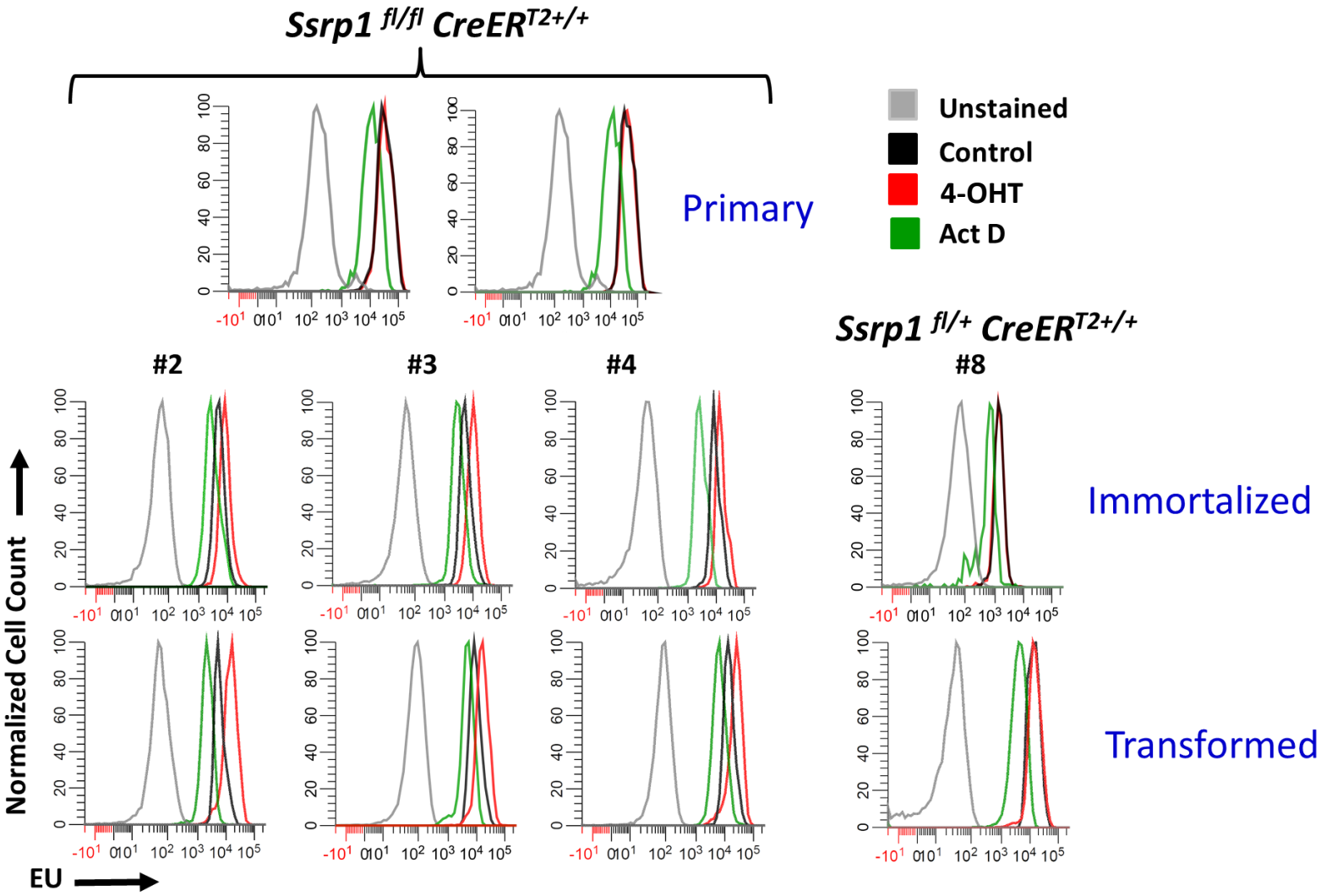

Figure S5 related to Figure 3. Effect of *Ssrp1* KO on EU incorporation in primary (Pr), immortalized (Im), and transformed (Tr) cells. Cells were treated for 15 min with EU 24 h after the end of the 5-day 4-OHT treatment. EU incorporation in control (black), 4-OHT (red) and Actinomycin D (ActD; green-treated Pr, Im, and Tr *Ssrp1*$^{fl/fl}$ *CreER*$^{T2+/+}$ (#2, #3, #4) and *Ssrp1*$^{fl/+}$ *CreER*$^{T2+/+}$ (#8) fibroblasts was measured using fluorescent activating cell sorting.

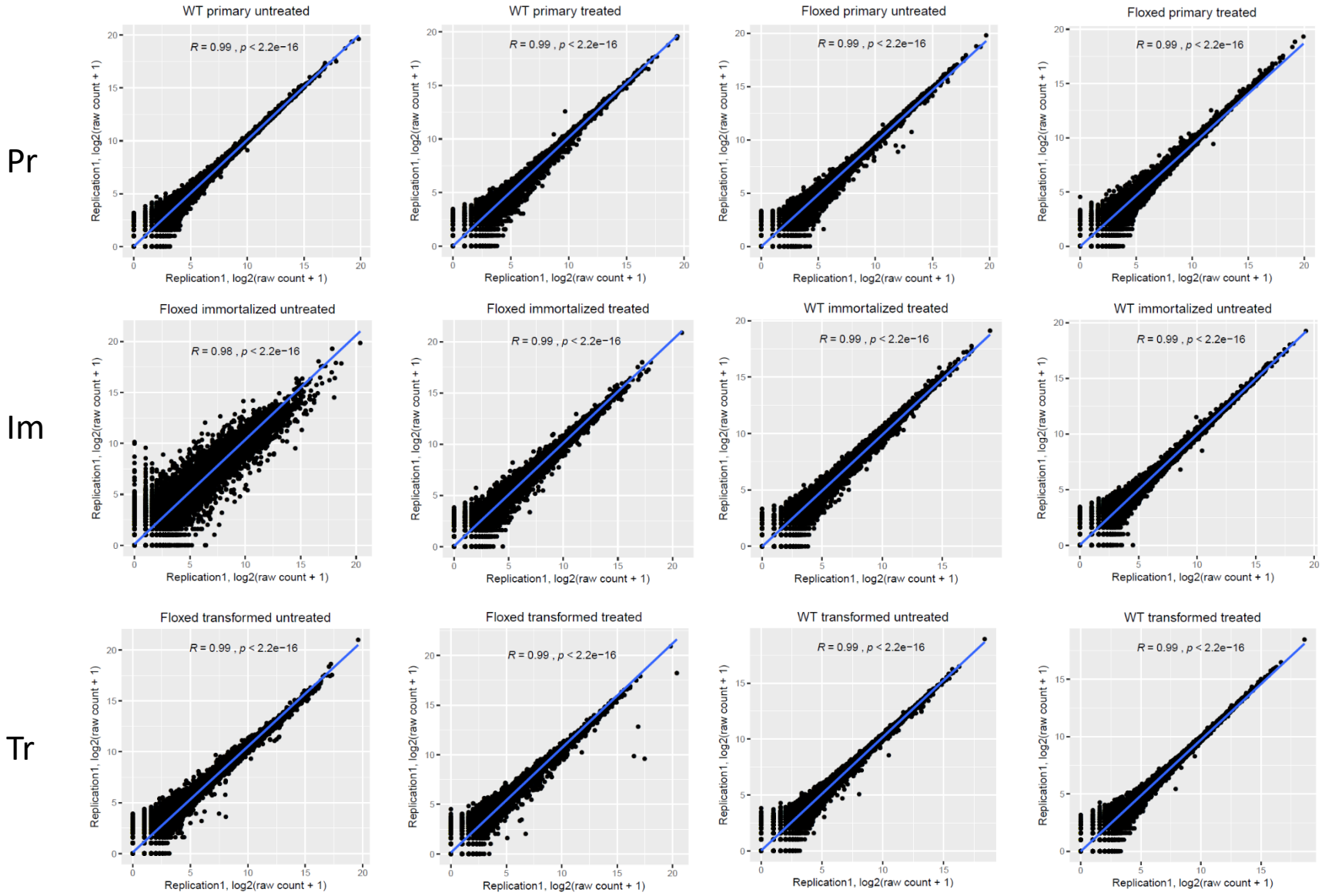

Figure S6 related to Figure 3. Correlation dot plots for RNA-seq replicates from mouse cells. Primary (Pr), immortalized (Im), and transformed (Tr) cells from *Ssrp1*$^{+/+}$*; CreER*$^{T2+/+}$ (WT) or *Ssrp1*$^{fl/fl}$*; CreER*$^{T2+/+}$ (floxed) mice were treated with 4-OHT or vehicle for five days. RNA-sequencing was performed for each condition for two replicates. R – Pearson correlation coefficient.

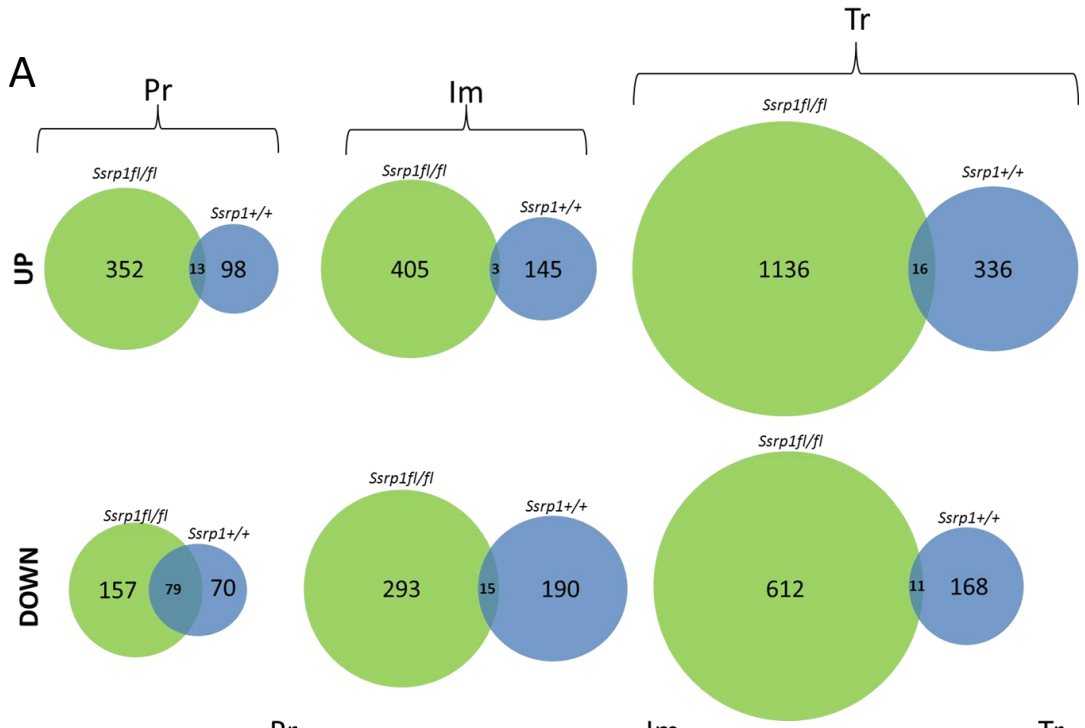

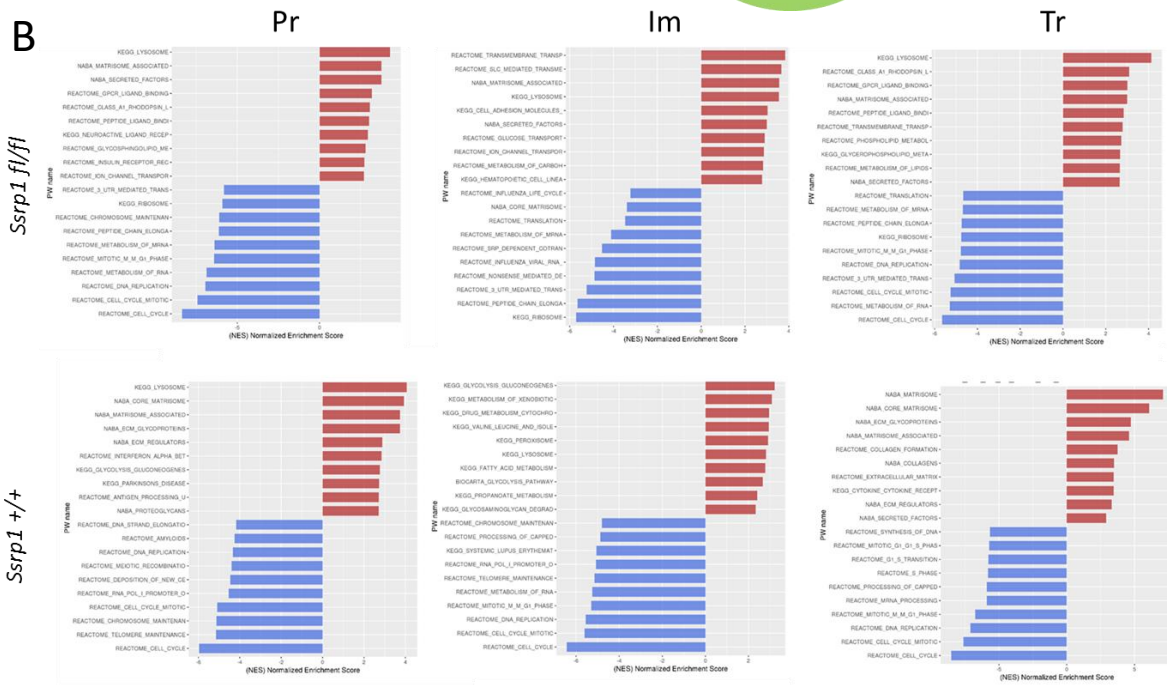

Figure S7 related to Figure 3. Analyses of RNA-seq of mouse cell samples. A. Venn diagram showing the number of shared differently up-regulated and downregulated genes (fold change >1.5 and adjusted p-value < 0.05) following 4-OHT treatment in primary (Pr), immortalized (Im), and transformed (Tr) cells from *Ssrp1*$^{+/+}$*; CreER*$^{T2+/+}$ (blue) and *Ssrp1*$^{fl/fl}$*; CreER*$^{T2+/+}$ (green) mice. B. Gene Set Enrichment Analyses of genes upregulated (red) or downregulated (blue) in primary (Pr), immortalized (Im), and transformed (Tr) cells from *Ssrp1*$^{+/+}$*; CreER*$^{T2+/+}$ (bottom row) or *Ssrp1*$^{fl/fl}$*; CreER*$^{T2+/+}$ (top row) mice in response to 4-OHT treatment.

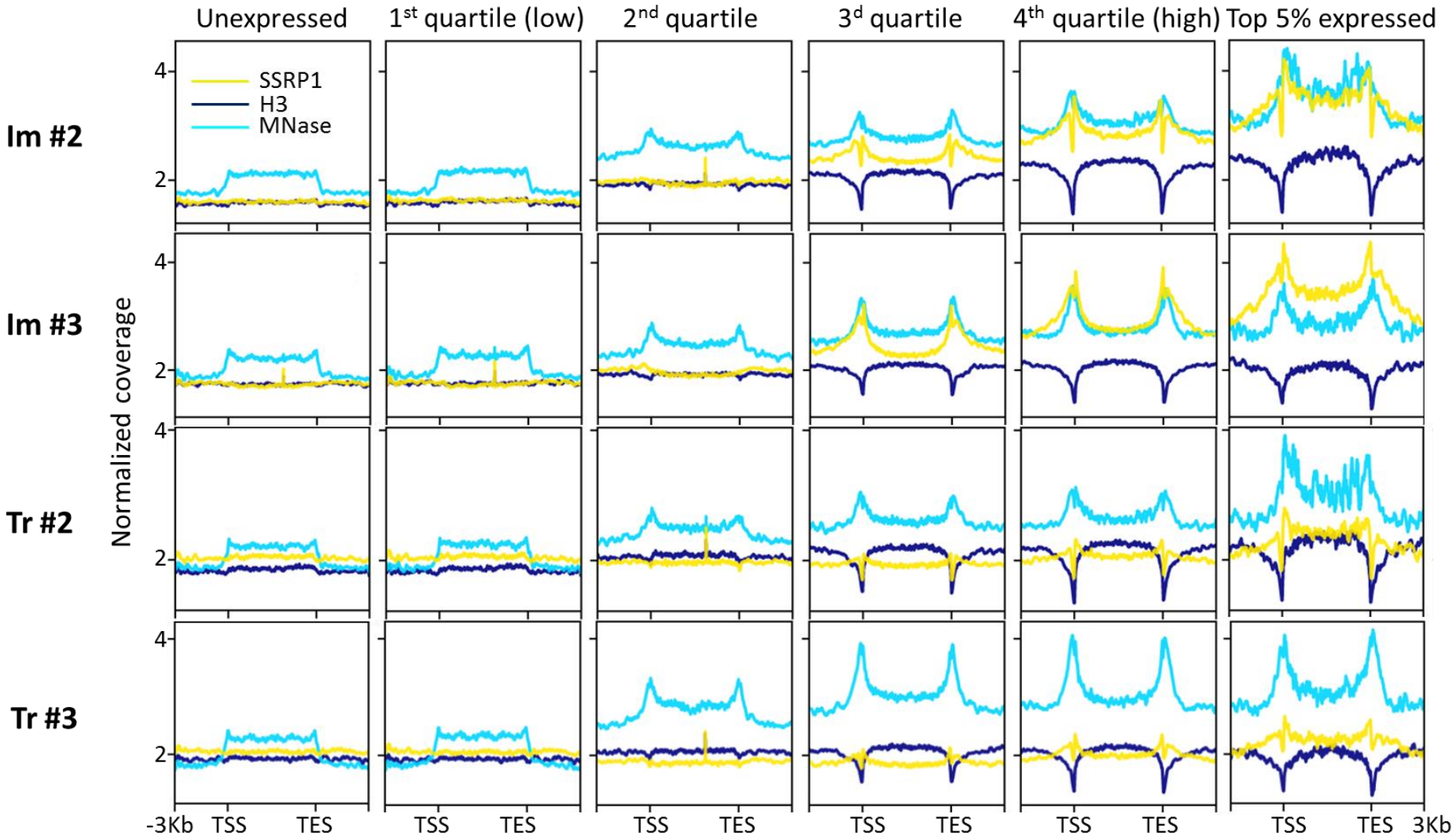

Figure S8 related to Figure 4. Average SSRP1 and histone H3 distribution profiles for two cell lines (#2 and #3) of immortalized (Im) and transformed (Tr) *Ssrp1*$^{fl/fl}$*; CreERT2*$^{+/+}$ MSFs depending on the level of gene expression (single end RNA-seq). The third profile represents the MNase-digested chromatin used for ChIP.

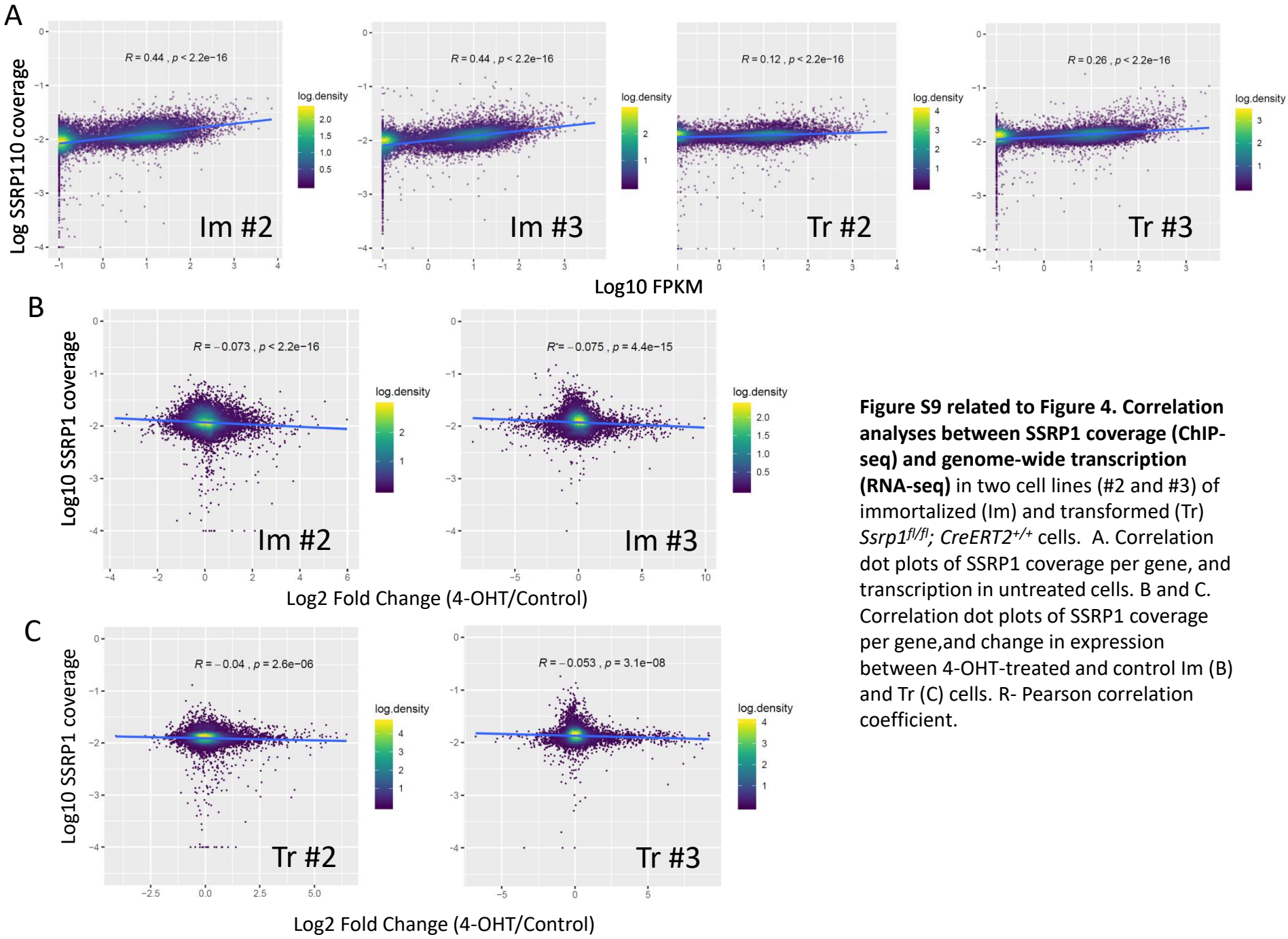

Figure S9 related to Figure 4. Correlation analyses between SSRP1 coverage (ChIP-seq) and genome-wide transcription (RNA-seq) in two cell lines (#2 and #3) of immortalized (Im) and transformed (Tr) *Ssrp1*$^{fl/fl}$*; CreERT2*$^{+/+}$ cells. A. Correlation dot plots of SSRP1 coverage per gene, and transcription in untreated cells. B and C. Correlation dot plots of SSRP1 coverage per gene,and change in expression between 4-OHT-treated and control Im (B) and Tr (C) cells. R- Pearson correlation coefficient.

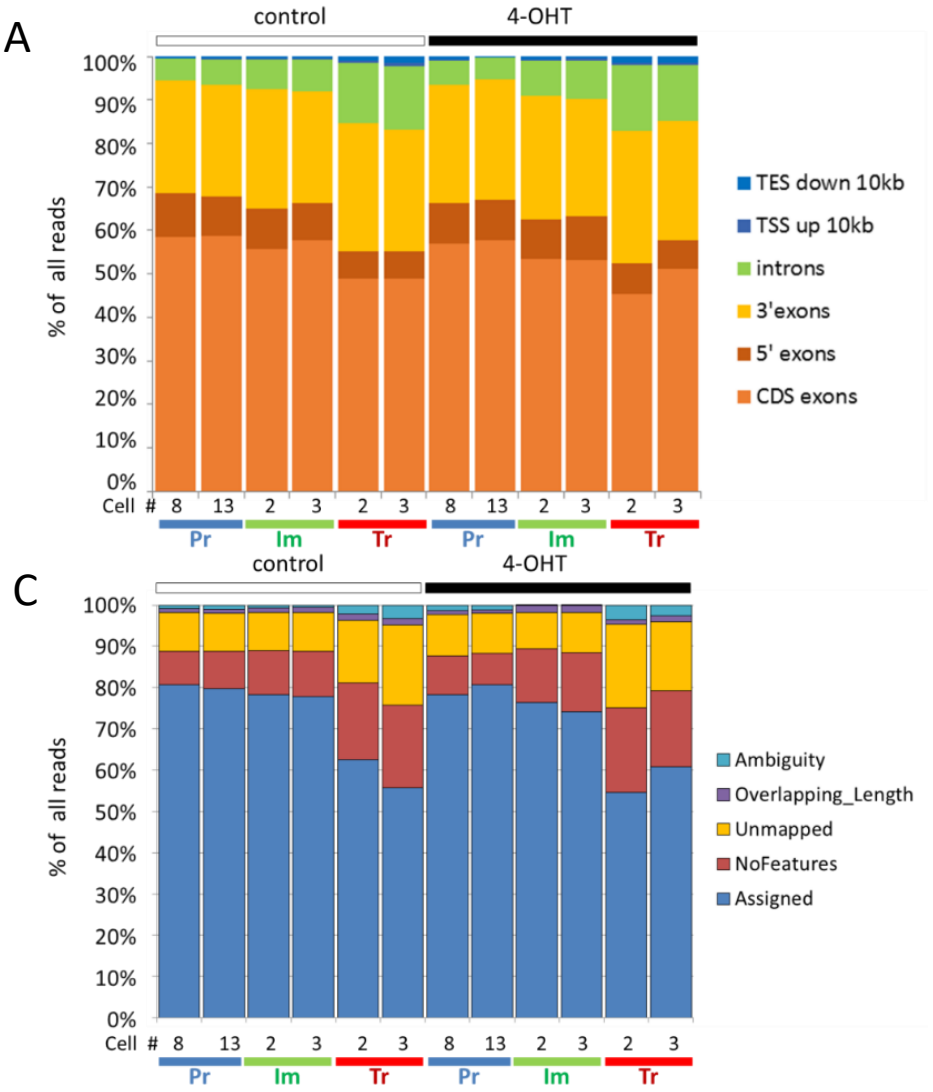

Figure S10 related to Figure 5. Increase of transcripts corresponding to introns or genomic regions with no features in cells upon immortalization and transformation detected by RNA-seq. A. Distribution of single end RNA-seq reads corresponding to different gene regions within individual samples: TES_down_10kb, read located within 10 kB downstream of the transcription end site; TSS_up_10kb, 10 kb upstream of the transcription start site; introns, within the intron of any gene; 3'UTR_Exons, within the last exon of a gene; 5'UTR_Exon, within the first exon of a gene; CDS_Exons, within all other exons of a gene. B,. Mean proportion of reads corresponding to introns within each category of samples +/- SDV. C. Distribution of single-end RNA-seq reads corresponding to annotated genomic features (Assigned) or not (NoFeatures) as well as reads with questionable annotations (Ambiguity, Chimera, Overlapping_Length) within individual samples. DE. Mean proportion of reads corresponding to regions with no features within each category of samples +/- SDV.

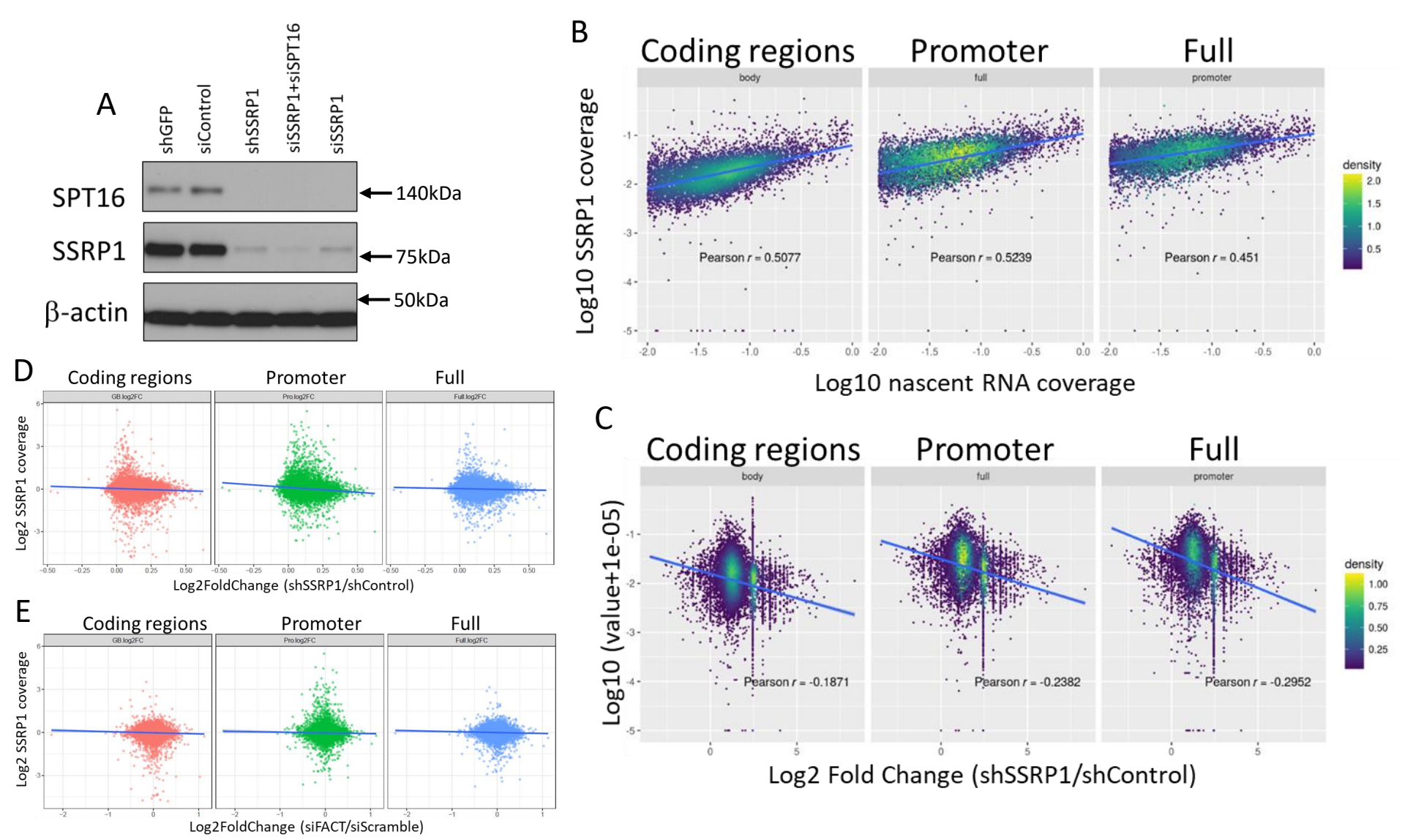

Figure S11 related to Figure 5. Correlation analyses between SSRP1 coverage (ChIP-seq) and genome-wide transcription in human fibrosarcoma cells (HT1080) cells. A. Immunoblotting of HT1080 protein extracts transduced or transfected with shRNA or siRNA constructs as indicated and probed with antibodies to SSRP1, SPT16 and beta-actin. B. Correlation between gene transcription (nascent RNA-seq) and SSRP1 enrichment analyzed at the coding regions (body), promoter regions (promoter), or both regions (full) in basal conditions. C. Correlation between SSRP1 coverage and changes in gene expression (RNA-seq) in cells transduced with shSSRP1 versus shControl. D. HT1080 cells were transduced with lentiviral shRNA to SSRP1 or GFP. Gene expression was measured five days after transduction and selection with puromycin using the Illumina Beads Array. E. HT1080 cells were co-transfected with siRNAs to SSRP1 and SPT16 or control siRNA. Gene expression was measured 72 h after transfection using the Illumina Beads Array.

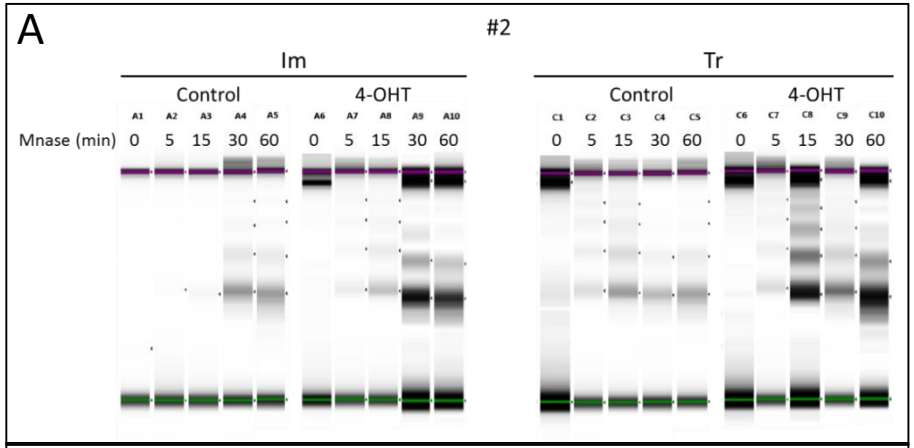

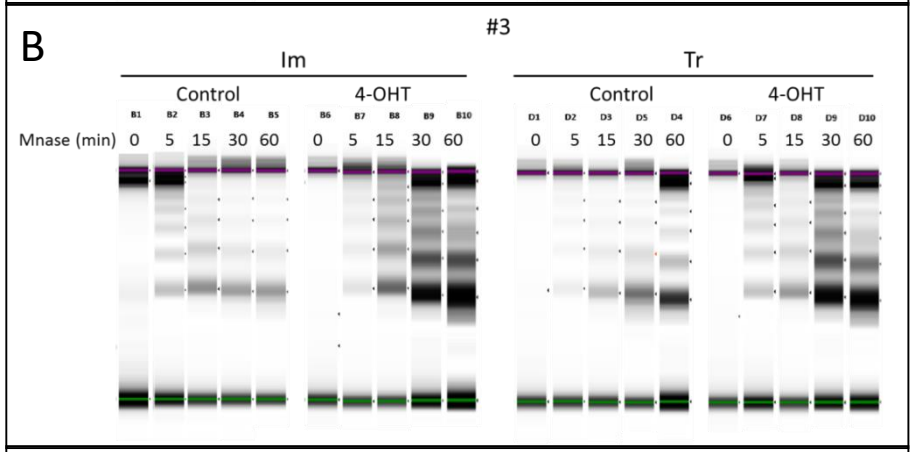

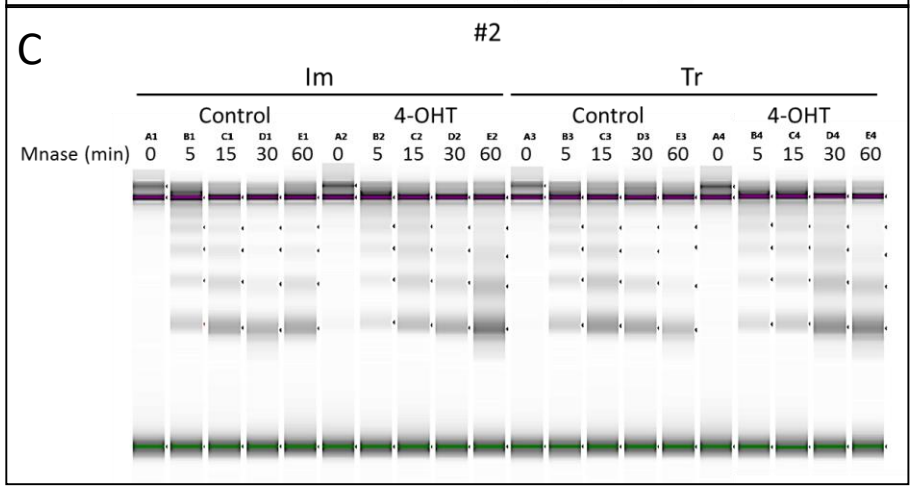

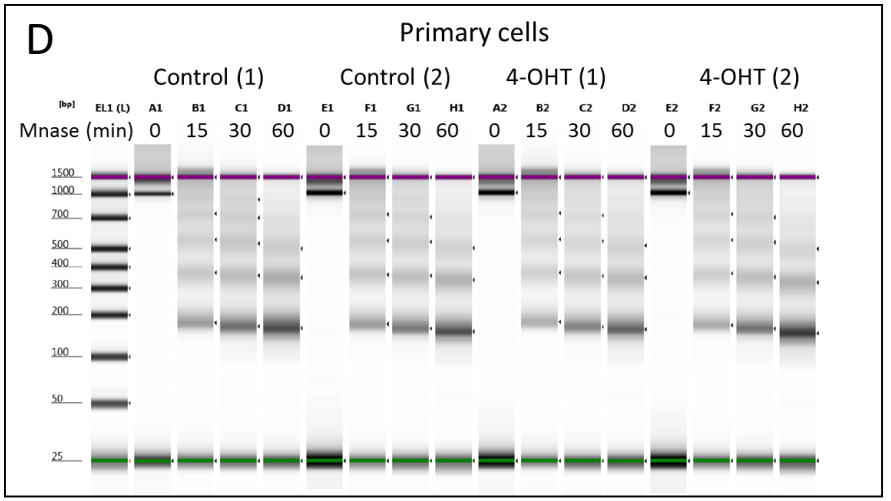

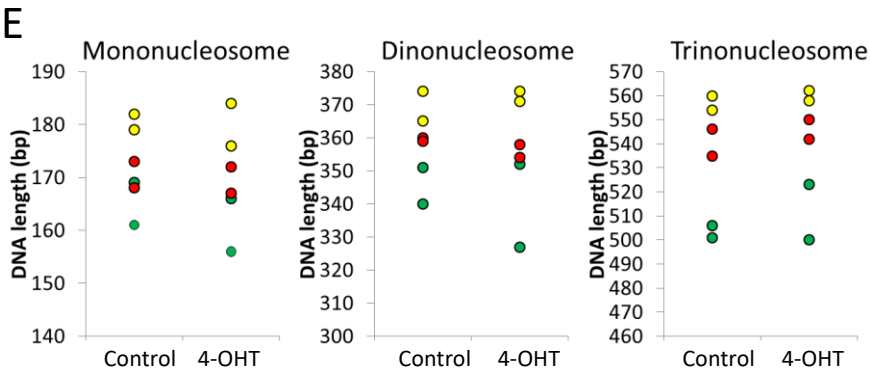

Figure S12 related to figure 6. MNase digestion of nuclei from cells with floxed *Ssrp1* treated with 4-OHT or vehicle for five days. A, B, C represent three independent experiments with immortalized (Im) and transformed (Tr) cells performed 24 h after the completion of 4-OHT treatment. . The same number of nuclei was used for each condition. D. Experiment done with primary cells (in two replicates). Isolated DNA was run on capillary electrophoresis (BioAnalyzer). Purple and green lines indicate positions of spike-in controls. E. Comparison of length of peaks corresponding to mono-, di- and trinucleosomes in primary cells before and after treatment with 4-OHT. Colors correspond to the time of treatment with MNase: yellow - 15 min, red – 30 min, green – 60 min. Two biological replicates are shown.

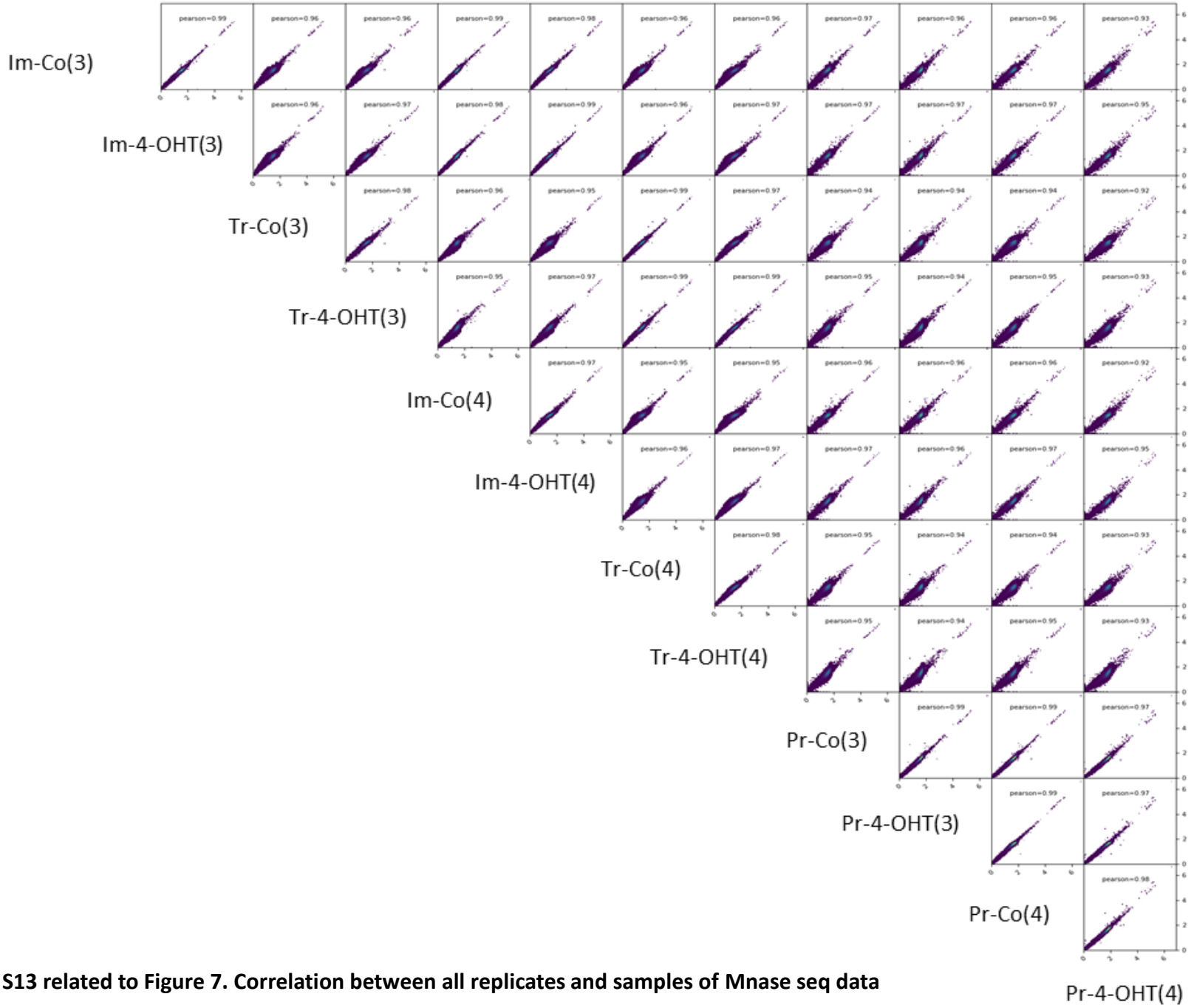

Figure S13 related to Figure 7. Correlation between all replicates and samples of Mnase seq data

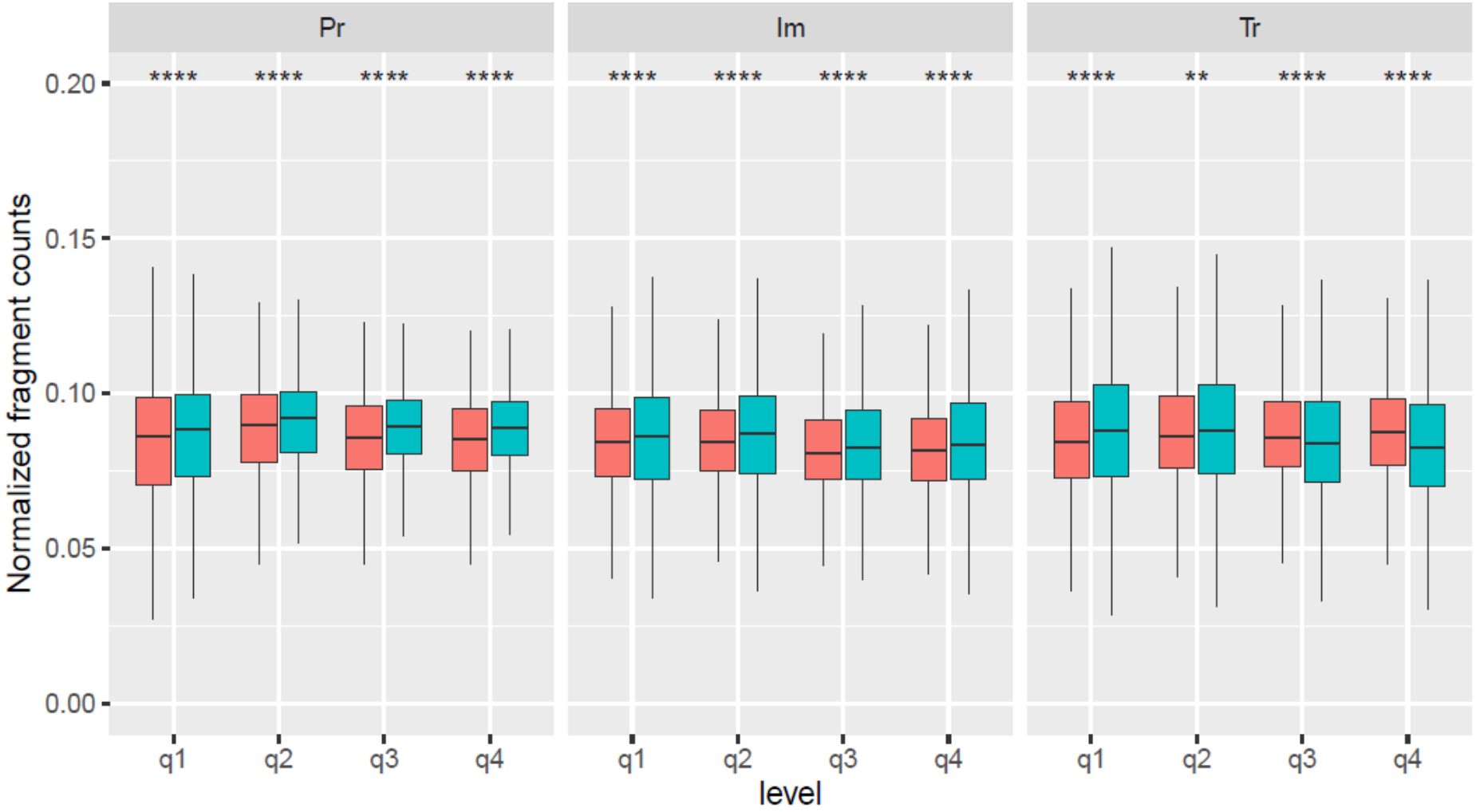

Figure S14 related to Figure 7. Comparison of nucleosome occupancy at coding regions of genes in Pr, Im and Tr cells based on their expression levels (q, quartile: 1 – the lowest, 4 – the highest). The number is calculated as: number of fragments in each gene/gene length, and all samples are normalized together with total number of assigned fragments. ** means $p < 0.01$; **** means $p < 0.0001$.

Transparent Methods

Reagents

Reagent	Source	Cat#	Application
Chemicals and kits			
Pierce® luciferase cell lysis buffer	Thermo Fischer scientific	16189	Cell lysis for protein extraction
Quick Start ™ Bradford 1x dye reagent	BioRad	500-0205	Measurement of protein concentrations
4–20% gradient precast gels	BioRad	3450028	Protein gel electrophoresis
PVDF membranes	BioRad	1620177	Immunoblotting
Western Lightning Plus-ECL	PerkinElmer	NEL104001	Enhanced luminescence
Hoechst 33342	Invitrogen	H3570	Staining of DNA, 1ug/ml
TRIzol	Thermo Fischer Scientific	15596026	Isolation of RNA
SuperScript™ First-Strand Synthesis System for RT-PCR	Thermo Fischer Scientific	11904018	First-strand synthesis for RT-PCR
Cell Titer Blue Reagent	Promega	G8081	Cell viability assay
Click-iT™ EdU Alexa Fluor™ 488/594 imaging kit	Thermo Fischer Scientific	C10337	DNA replication assay
4-hydroxytamoxifen	Millipore Sigma Aldrich	H7904	Induction of Ssrp1 deletion
Tamoxifen	Millipore Sigma Aldrich	T5648	Induction of Ssrp1 deletion
Caspase-3 substrate (Ac-DEVD-AMC)	Enzo Life Sciences, cat# ALX-260-031-M005	ALX-260-031-M005	Apoptosis assay
RNase A	Roche	11119915001	Cell cycle assay
Propidium Iodide	Calbiochem	537059	Cell cycle assay
EU Click-iT™ RNA Alexa Fluor™ 488 Imaging Kit	Thermo Fischer Scientific	C10329	General transcription
Micrococcal nuclease (MNase)	NEB	M0247S	Mnase Assay
p35 plates with glass bottom	Mattek Corp	P35G-1.0-14-C	FRAP assay

Antibodies

SSRP1 mouse monoclonal 10D1	BioLegend Inc.	609702	IB dilution 1:3000, IF dilution 1:200
SPT16 monoclonal mouse 8D2	BioLegend Inc.	607002	IB dilution 1:2000, IF dilution 1:200
p53	Millipore Sigma Aldrich	PAb421	IB dilution 1:300
H-Ras rabbit polyclonal	Santa Cruz	sc-520	IB dilution 1:1000
beta-actin mouse monoclonal	Millipore Sigma Aldrich	A3854	IB dilution 1:20000
Anti-α tubulin	Millipore Sigma Aldrich	T9026	IF staining, dilution 1:200
Secondary anti-mouse Alexa Fluor® (488 and 594)	Life Technologies	A-11062 and 11001	IF staining, dilution 1:500
Primers			
SSRP1-Mm01268569_m1	Applied Biosystems	SSRP1-Mm01268569_m1	Primeres for qPCR (mouse)
SUPT16 Mm01314632_m1	Applied Biosystems	SUPT16 Mm01314632_m1	Primeres for qPCR (mouse)
GAPDH Mm99999915_g1	Applied Biosystems	GAPDH Mm99999915_g1	Primeres for qPCR (mouse)
TaqMan gene Expression Master Mix	Thermo Fischer Scientific	4369016	Master-mix for qPCR

Cells

Mouse skin fibroblasts (MSF) and their immortalized and transformed variants were generated as described [22]. Human fibrosarcoma HT1080 cells were originally from ATCC, they were not authenticated, but these are the same cells as we used in our other published studies [7] and their gene expression profiles and ChIP-seq profiles for SSRP1 is highly reproducible (98-99% correlation). Cells were cultured in DMEM (different vendors) with 10% (MSF cells and their variants) or 5% Fetal Bovine Serum (FBS, different vendors) and antibiotics.

Phenotypic characterization of consequences of Ssrp1 KO in mouse cells

MSFs (1-2 x 106 cells) were plated in 150 mm plates. The next day, cells were treated with 2 μM 4-OHT for 96 h (Pr) or 120 h (Im and Tr). The medium was replaced every 48 h with fresh 2 μM 4-OHT. At the end of treatment, both treated and untreated cells were trypsinized and re-plated for further experiments. Ssrp1 excision was confirmed using western blotting or genomic PCR as described [22]. Experiments were performed in triplicate and repeated at least twice.

Cell viability was assessed five days after plating of 5 x 10^5 cells per well of a 6-well plate using Cell Titer Blue Reagent (Promega). Cell cycle analysis was performed as previously described [11]. For 3D colony growth, 1 x 105 cells were mixed with 0.3% agarose and plated over a layer of 0.5% agarose in a 6-well plate. The two layers were covered with medium and

incubated at 37°C in 5% CO2 for 2 to 4 weeks or until visible colonies appeared. Colonies were stained with 0.01% crystal violet in 10% ethanol and counted in 10 random fields per well.

Cell death was measured after plating 2 x 10^4 cells in the wells of 96-well plates in triplicate. The next day, the medium was removed and 20 µL lysis buffer (50 mM HEPES, 0.1% CHAPS, 2 mM dithiothreitol, 0.1% Nonidet P-40, 1 mM EDTA, and 1% protease inhibitor) and 20 µL caspase assay buffer (100 mM HEPES, 10% Sucrose, 0.1% CHAPS, 1 mM EDTA, 2 mM dithiothreitol, and 50 µM Caspase-3 substrate) were added. Fluorescence (excitation 380 nm, emission 430 - 460 nm) was measured at 0, 5, and 24 h.

DNA replication was measured 24 h after plating of 5X10^4 cells per well of a 6 well plate by incubation of cells with 15 µM EdU for 2 h. General transcription was measured 24 h after plating of cells by incubation with 1 mM of EU for 40 min or 3 h at 37°C.

All flow cytometry was measured on the BD LSRII machine using FACSDiva software and analyzed using WinList software.

The MNase assay was performed as described [36] 24 h after the end of the 4-OHT treatment nuclei was isolated from 2 x 10^7 cells per condition and incubated with 200u/ml of MNase (New England BioLabs, cat#M0247S) for different amount of time. For each reaction, 10 µl DNA was submitted for Bioanalyzer QC analysis.

For the FRAP assay, cells were plated into 35-mm glass bottom plates (Mattek Corp., cat# P35G-1.0-14-C). The assay was performed 24 h after plating using a Leica DMi8 inverted microscope and TCS SP8 laser scanner with Leica Application Suite X (LAS-X) acquisition software (four pre-bleach images with 433 ms intervals and eight bleaches with 100% 522 nm laser power followed by 250 post-bleach measurements every second). Data were accumulated for 15 to 20 cells. All measurements were normalized by the average pre-bleach fluorescence intensity.

Immunoblotting

Standard immunoblotting methods were used. Antibodies and dilutions are listed above.

Immunofluorescence staining

Cells were fixed with 4% paraformaldehyde, and staining was performed as previously described [58]. The antibodies are listed in Table 1. Images were acquired using a Zeiss Axio Observer A1 inverted microscope with an N-Achroplan 100×/1.25 oil lens and a Zeiss MRC5 camera with AxioVision Rel.4.8 software. Image analysis and quantitation were done using ImageJ.

RT-qPCR

Total RNA was isolated using TRIzol reagent. First-strand cDNA (30 µL) was synthesized from 500 ng RNA using the SuperScript™ First-Strand Synthesis System. qPCR was performed using 1 µl first-strand cDNA with primers and master mix purchased from Applied Biosystems and the default parameters of the 7900HT sequence detection system (ABI PRISM; Applied Biosystems). To compare gene expression levels between samples, the threshold cycle (CT) value was normalized using the mean CT for the reference gene, GAPDH. The normalized mRNA levels were defined as ΔCT = CT (mean for test gene) − CT (mean for the reference gene). The final data were expressed as the fold difference between the test sample and the control sample, which was defined as 2-(ΔCT treated with 4-OHT - ΔCT control).

High Throughput Whole Genome Methods

RNA-Sequencing of mouse cells

For the RNA sequencing data shown in Figures 3, 4, 5, S6, S7, and immortalized and transformed cells # 3 on Fig. S8 and S9, RNA was isolated using Monarch Total RNA Kit (T2010S, New England BioLabs). The total RNA quality was assessed using an Agilent Bioanalyzer. RNA with an overall RIN score >9 was used. RNA was depleted of ribosomal transcripts using the RiboErase kit (Roche). RNA libraries were prepared from 500 ng RNA using the Kapa RNA HyperPrep kit (Roche). All RNA libraries were sequenced using massively parallel sequencing (Illumina, NovaSeq) with 100 base pair paired-end reads. Two independent RNA-seq experiments were performed.

For the RNA sequencing data shown in Figures S10 and immortalized and transformed cells #2 on Fig. S8 and S9 RNA was isolated using TRIZOL reagent (Invitrogen, Life Technologies). The total RNA quality was assessed using an Agilent Bioanalyzer. RNA with an overall RIN score >9 was used. RNA was depleted of ribosomal transcripts using the RiboZero Gold kit (Illumina). RNA libraries were prepared from 1000 ng RNA using TruSeq Stranded RNA kit (Illumina). All RNA libraries were sequenced using massively parallel sequencing (Illumina, NextSeq) with 75 base pair single-end reads. Two independent RNA-seq experiments were performed.

RNA-Sequencing of human HT1080 cells

HT1080 cells were infected with lentiviruses produced using psi-LVRU6MP encoding shRNA to SSRP1, clone HSH017741-8-LVRU6MP(OS396821) (cat no. CS-HSH0177741-8-LVRU6MP) or control clone CSHCTR001-LVRU6MP(OSNEG20) (cat no. CSHCTR001-LVRU6MP) from GeneCopoeia. Cells were selected with puromycin for three days and then counted. RNA was isolated using the Monarch Total RNA Kit (T2010S, New England BioLabs). A 1:1000 dilution of ERCC RNA Spike-in Mix1 (Life Technologies) was added to 100 ng total RNA at a ratio corresponding to the number of input cells used for RNA extraction. RNA was depleted of ribosomal transcripts using the RiboZero Gold kit (Illumina). RNA libraries were prepared from 1 μg total RNA using TruSeq Stranded Total RNA kit (Illumina) according to the manufacturer's instructions. The resulting pool was loaded into the appropriate NextSeq Reagent cartridge, for 75 single-end sequencing, and sequenced using the NextSeq500 following the manufacturer's recommended protocol (Illumina).

Chromatin Immunoprecipitation (ChIP) and sequencing

ChIP-Seq samples were prepared from mouse cells using the SimpleChIP Kit (cat no. 9003, Cell Signaling Technology). Immunoprecipitation was performed using the mouse monoclonal 10D1 anti-SSRP1 antibody (10 μg/IP; cat no. 609702, BioLegend, Inc). The histone H3 (D2B12)XP rabbit monoclonal antibody provided in the kit was used as a positive control. DNA isolated after MNase digestion was used as the input DNA.

For the ChiP-Seq, 2 ng chromatin-immunoprecipitated DNA was used to generate the library for next-generation sequencing using the ThruPLEX DNA seq kit (Rubicon Genomics, Inc.) according to the manufacturer's instructions. The DNA libraries were quantitated using the KAPA Biosystems qPCR kit and pooled in an equimolar fashion. Each pool was denatured and diluted to 2.4 pM with 1% PhiX control library. The resulting pool was loaded into the

appropriate NextSeq Reagent cartridge for 75 paired-end sequencing and sequenced on a NextSeq500 following the manufacturer's recommended protocol (Illumina).

Micrococcal nuclease (MNase) sequencing

Cells were untreated/treated with 4-OHT for 96 hours. $2X10^7$ nuclei per sample were used for MNase digestion. First, conditions were titrated using transformed cells as described [53] and then used for all other cells. MNase was purchased from Worthington Biochemical Corp (Cat# LS004797). The sequencing libraries were prepared with the HyperPrep Kit (KAPA BIOSYSTEMS), from 1ug DNA. Following manufacturer's instructions, the first step repairs the ends of the DNA fragments and a single 'A' nucleotide is then added to the 3' ends of the blunt fragments. Indexing adapters, containing a single 'T' nucleotide on the 3' end of the adapter, are ligated to the ends of the dsDNA, preparing them for hybridization onto a flow cell. Adapter ligated libraries are amplified by 3 cycles of PCR, purified using AMPureXP Beads (Beckman Coulter), and validated for appropriate size on a 4200 TapeStation D1000 Screentape (Agilent Technologies, Inc.). The DNA libraries are quantitated using KAPA Biosystems qPCR kit, and are pooled together in an equimolar fashion, following experimental design criteria. Each pool is denatured and diluted to 300pM with 1% PhiX control library added. The resulting pool is then loaded into the appropriate NovaSeq Reagent cartridge for 50 cycle paired-end reads and sequenced on a NovaSeq6000 following the manufacturer's recommended protocol (Illumina Inc.).

Analyses of NGS data

Raw reads that passed the quality filter from Illumina Real Time Analysis (RTA) software were mapped to the latest reference genome (hg38 for human and mm10 for mouse samples, respectively) using Tophat2 [54]. The gene expression quantitation was generated using the Subsread package [55] with GenCode for differential expression analysis using DESeq2 [56]. Pathway analysis was done using GSEA [57] with C2 curated gene sets in MSigDB. ChIP-Seq reads were mapped to reference genomes using bwa [58], and the narrow peaks were identified by MACS2 [59] using the input DNA as a control. Because SSRP1 is a protein that occupies the entire gene, we only used non-overlapping protein-coding genes (with NM prefix in RefGene) to study the relationship of gene expression with SSRP1 coverage. Genes were grouped into different categories according to the RPKM/FPKM values generated using the edgeR [60] Bioconductor R package. The big wiggle files and SSRP1 profiles for the whole gene and around the TSS were generated using the deepTools suite [61]. The correlation coefficients and p-values between RNA expression and SSRP1 coverage were calculated using R statistical software. For human RNA-Seq samples with ERCC spike-in, the normalization factors were determined using the loess normalization function from affy [62] Bioconductor package before differential gene analysis using DESeq2.

For statistics of FACT distribution at different genomic regions (genes or inter-genic regions), the numbers of non-duplicate reads with mapping score greater than 20 are counted using featureCount. The total number of reads of the two samples (Im and Tr) are scaled to the median value, and the average coverage of each genomic region is calculated by the scaled reads count divided by the region length. Genes with reads count > 10 in both samples are considered as expressed, otherwise not expressed. Only Refseq genes that do not overlap with any other genes were used. For intergenic regions, any gene regions with 500bp extension both sides were

excluded. Paired-end reads of SSRP1 ChIP-Seq data (gene or intergenic regions) were normalized by region length and total number of reads in all regions.

For MNase-seq analysis raw reads passed quality filter from Illumina RTA were mapped to mouse reference genome (mm10) after quality control check using FASTQC and the fragment insert size distributions were inspected to identify potential experimental problems. The big wiggle files are generated using read pairs of insert size between 135 to 200bp with PCR duplicates and low quality (map quality < 20) removed by deepTools. The big wiggle files are FPKM normalized and coverage profiles are generated accordingly.

Animal experiments

All animal experiments were conducted according to a protocol approved by the Institute Animal Care and Use Committee at Roswell Park Comprehensive Cancer Center. The facility has been certified by the American Association for Accreditation of Laboratory Animal Care in accordance with the current regulations and standards of the U.S. Department of Agriculture and the U.S. Department of Health and Human Services.

For in vivo tumor growth, $1x10^6$ cells (Im or Tr #3) were injected subcutaneously into both lateral flanks of ten 6-week-old female SCID (C.B-Igh-1b/IcrTac-Prkdcscid) mice (n = 20). In mice inoculated with immortalized cells, only one tumor appeared during three months of observation. Tumors were visible in most Tr-inoculated mice 3 to 5 days after inoculation. Mice were randomly divided into treatment and control groups (n = 10) 48 h post-inoculation. The treatment and control groups received 1 mg tamoxifen in 100µL 5% ethanol or plain 5% ethanol i.p. following a 3 days on/1 day off schedule, respectively. Treatment was continued until the control tumors reached 1 cm3.

Statistical analysis

Data were compared between the control and treated groups using the unpaired t-test (Mann-Whitney test). Analyses were conducted using GraphPad Prism 7.03 and all p-values were two-sided.